# Thermal Analysis Of Decomposition Reactions Of Aspartic And Glutamic Acids In Potassium Chloride Matrix

By

Praveen Kumar Bandarupalli

Submitted in Partial Fulfillment of the Requirements

for the Degree of

Master of Science

in the

Chemistry

Program

YOUNGSTOWN STATE UNIVERSITY

December, 2013

Thermal Analysis of Decomposition Reactions of Aspartic and Glutamic acids in Potassium Chloride Matrix

Praveen Kumar Bandarupalli

I hereby release this thesis to the public. I understand that this thesis will be made available from the Ohio LINK ETD Center and the Maag Library Circulation Desk for public access. I also authorize the University or other individuals to make copies of this thesis as needed for scholarly research.

Signature:

*Praveen Kumar Bandarupalli*, Student Date

Approvals:

*Dr. Ganesaratnam K. Balendiran*, Thesis Advisor Date

*Dr. Russell J. Moser*, Committee Member Date

*Dr. Sherri R. Lovelace-Cameron*, Committee Member Date

*Dr. Salvatore A. Sanders*, Associate Dean of Graduate Studies Date

# Abstract

The Thermal analysis of aspartic and glutamic acid samples in potassium chloride (KCl) matrix at 10 % (w/w) interval ratios of amino acid and KCl was investigated by using thermogravimetry and differential scanning calorimetry in order to study their decomposition. The samples were subjected to a heating rate of 10 °C/min under nitrogen atmosphere. These thermogravimetric data were analyzed by a software PSI (Poly Software International) Plot version 9.5 to determine the kinetic parameters like activation energy ($E_a$), pre-exponential factor ($A$) and order of the reaction ($n$) for the reactions occurring in each sample. An interesting trend was observed in the kinetic parameters as the percentage of potassium chloride varied and this observation can be attributed to the potassium ion interaction with amino acid molecules to form complexes. The results obtained in this study correspond to the reactions occurring in these samples at higher temperatures, as proposed in the literature, but provide further insight to their reaction pathways.

## Acknowledgements

It is a pleasure to thank everyone who supported me in completion of this thesis. I would like to express my deepest gratitude to my thesis advisor Dr. Ganesaratnam K. Balendiran for his guidance, continuous support and encouragement throughout the research. My sincere thanks must go to Dr. Russell J. Moser for all his patience, immense knowledge and for being part of my thesis committee. I should acknowledge Dr. Balendiran and Dr. Moser for the valuable discussions from the beginning of this project, which helped me in completing the thesis. Special thanks to Dr. Sherri R. Lovelace-Cameron for being a supportive graduate advisor from the beginning of my graduate program and also for readily accepting to be part of my thesis committee, in a short notice.

I would like to thank Dr. Malkhey Verma for helping me in my thesis with FFT Filter Smoothing of curves using MATLAB, Mr. Raymond E. Hoff for helping me with the instruments and Mr. Timothy Styranec for all the help.

Heartfelt thanks to my fellow lab mates and students for being nice to me. I am grateful to my family especially my sister Sruthi Bandarupalli and my friends and fellow graduates Srivani Kalapala, Krishna Vemulapalli, Leela Krishna, Prudhvidher Reddy and Sandeep Kakkerla for their help, unconditional love, support, concern and encouragement.

I would also like to thank Youngstown State University, Department of Chemistry and School of Graduate Studies and Research for all the financial support.

# Table of Contents

# List of Figures

# List of Tables

# Introduction

Amino acids are the fundamental building blocks and essential structural units of peptides and proteins. They play several important biological roles and act as the primary substrates for various enzymatic reactions. In addition, they are widely used in the food, agriculture, cosmetics, and pharmaceutical industries. Amino acids can remain stable even in diverse conditions which includes temperature and pressure. They can transform into large biological molecules under certain conditions. For example, a study reported the thermal stability, decomposition and transformation of amino acids [1].

In naturally occurring proteins, twenty amino acids are commonly found and are referred to as standard amino acids. When two amino acid molecules are linked, they form a dipeptide. In peptides, the amino acids are linked together by the functional amino and carboxyl groups in –CO–NH– peptide bonds forming a chain. In the crystalline state, the functional groups of amino acids are held together by the hydrogen bonds. Such compounds are capable of undergoing solid-state phase transitions. The solid state of amino acids shows various structural variations which can be a simple model for conformational dependent biochemical processes [2]. Because of the hydrogen bonding between the $COO^-$ and $NH_3^+$ groups which are linked to the same α-carbon atom, the solid α-amino acids have high melting points. The general thermal behavior can be determined by such dipolar ion structure. The thermal behavior of α-amino acids between and within classes can be differentiated by the effect of the side-chain. The phase transitions of these compounds are related to a conformational change in the alkyl chain and to the appearance of a completely different hydrogen bond network [3].

Most of the studies are done on amino acids, which can be used as models to understand the characteristics and reaction mechanisms of the complex molecules like peptides and proteins. The reactions of small peptides in their solid state are not given much attention whereas the solution reactions are well-characterized. It is very important to understand the solid-state behavior of small peptides because of their increasing use as pharmaceuticals [4]. The major concern for pharmaceuticals is the stability of products and this problem remains a major challenge for the chemists and the pharmaceutical industry. The solid dosage forms have to be made to achieve an acceptable shelf life in order to overcome the instability problems in aqueous solutions [5, 6]. Solid formulations often possess greater long-term stability than liquid formulations because the observed reaction rates of chemical degradation are dramatically slower in the solid state [5, 7]. The loss of active ingredient may occur due to lack of stability [4]. Moreover, the stability problems for liquid formulations that occur due to mechanical stress during shipping and handling can be avoided by the solid dosage forms [5]. The solid state reactions are classified as physical transformations or chemical reactions. The polymorphic transitions and desolvations which are characterized by the changes in crystal structure without the modifications of the component molecules are considered as physical transformations whereas, the rearrangements, decompositions and photochemical reactions are considered as chemical reactions of the solid state. Thermal analysis may help in the general understanding of the solid state chemistry of small peptides [4].

The physical measurements of thermal decomposition process for organic compounds can be provided by thermal analysis of solid phases but gives no chemical

information on the process being studied. The products of thermal decomposition can be identified by thermal analysis of organic compounds [8, 9]. During the thermal reactions of amino acids, they can undergo dehydration, decarboxylation and deamination losing small molecules like water, carbon dioxide and ammonia respectively over a wide temperature span forming reactive dipeptides which makes the quantitative measurements difficult [8, 10, 11]. These dipeptides are non-detectable intermediates due to their high thermal reactivity and low volatility and thus, they remain in thermal zone until they further react [11]. Moreover, when the crystalline solids are heated to relatively high temperature, they undergo decomposition over a range of several degrees. It is difficult to assign identity or confirm their structure based on the decomposition points as a characteristic property. Thus, structure can be assigned by further identification based upon the melting points of amino acids [10]. Melting is a first order phase transition from the crystalline solid phase to the liquid phase, without any change in the chemical composition. The melting parameters can be used as unique material properties for identification and characterization of crystalline materials because they provide a good deal of information about the characteristics of the crystalline material [12].

Thermal analysis can provide useful information on the characterization of some organic compounds. Thus, differential thermo-analytical methods are the most appropriate techniques for characterizing amino acids in the solid state. Thermal analysis is a very valuable tool that can be used in the broad field of physico-chemical and analytical studies of amino acids, due to its basic characteristics like simple procedures, speed of operation and ability to be used in direct identification of compounds [10]. The studies on thermodynamics, structure and conformations of amino acids and peptides of

small size are necessary for consequent simulation of the properties of more complex polypeptide and protein compounds [13]. In this study, the thermal analysis of amino acids was done by using thermogravimetry and differential scanning calorimetry. The thermogravimetric data were used to calculate the kinetic parameters like activation energy ($E_a$), pre-exponential factor ($A$) and order of the reaction ($n$) for the reactions occurring in the samples.

The amino acids used in our study are Aspartic acid (Asp) and Glutamic acid (Glu). In general, these two standard amino acids are acidic amino acids and they have side chains with carboxylate groups. At physiological pH, the side chains of aspartic acid and glutamic acid are negatively charged and thus, they are often referred to as aspartate and glutamate.

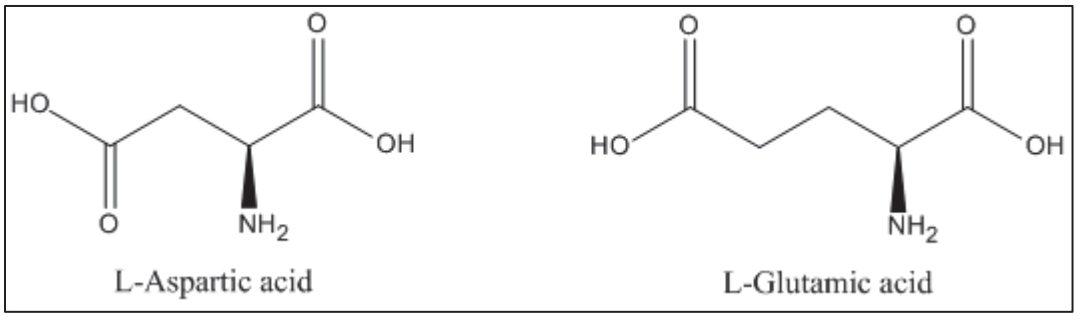


**Figure 1: Structures of L-Aspartic acid and L-Glutamic acid [49]**

## Aspartic Acid (Asp):

Aspartic acid is a non-essential amino acid and a biologically active substance. Its residues are widely found in various proteins. It is the simplest acidic amino acid made from glutamic acid by enzymes using vitamin B6 and plays important physiological roles in the urea cycle and DNA metabolism. It can also be prepared chemically or by fermentation of carbohydrates [14]. Aspartic acid is a proteinogenic α-amino acid which

plays a crucial role as an intermediate in generating other amino acids and biomolecules. As a component of protein molecules, it helps in maintaining their solubility and ionic character. It is also involved in protein active sites of the serine protease trypsin forming part of the catalytic triad and in biological systems like bacteriorhodopsin; it is the key functional group in proton-transfer processes. Aspartic acid has a polar group which can act as a proton acceptor or donor and thus increases the possible combinations of intramolecular interactions between different functional groups resulting in the formation of various conformers with low energy and stabilized with a network of hydrogen bonds involving the amino group and two carboxyl groups [15]. Aspartic acid provides resistance to fatigue by acting as an excitatory neurotransmitter in the brain. It can protect from the adverse effects of radiation by acting as a significant immunostimulant of the thymus. Because of the important roles of aspartic acid and its derivatives in biological processes, and due to its relatively non-toxic nature, many studies have been carried out to elucidate the pharmacological and therapeutic roles of aspartic acid. The structural information of aspartic acid and its residues is important to study their reaction mechanisms in biological processes [14].

The potassium, magnesium or calcium salts of Aspartic acid are widely used for mineral supplementation. Aspartic acid is a fragment of biologically active substances which are employed in Agriculture [16]. Polyaspartate, which is the condensation polymer of aspartic acid, keeps fertilizer available for longer periods of time and thus, increases the nutrient level in plants [17]. By heating the aspartic acid in solid state for several hours at high temperatures, poly aspartic acids with low molecular weight are prepared commercially. Polyaspartate is biodegradable and can be used as an anti-scalant,

or a dispersant, or a super-absorber [18]. Aspartic acid along with other amino acid phenylalanine is a part of aspartame, a new natural sweetener, which is probably safe to all except phenylketonurics and may also have long term effects on many brain neurohormones. Thus, it has wide applications in pharmaceutical, food and chemical industries [4].

According to the earlier thermal studies on Aspartic acid, performed by using thermogravimetric analysis and differential scanning calorimetry, it was determined that the two-stage amino acid polycondensation occurs. In the first stage, polyaspartic acid (PAA) is formed due to autocatalytic chain growth and in the second stage, polysuccinimide (PSI) is formed due to dehydration and polymer-analogous transformation [19, 20, 21].

**Glutamic Acid (Glu):**

Glutamic acid is a non-essential amino acid. In the body, glutamic acid or glutamate is synthesized from Arginine, Proline and Ornithine and is converted to glutamine [22]. Glutamic acid and its derivatives have several commercial applications. They are incorporated in drugs for treating epilepsy, ulcers, hypoglycemia, Parkinson's, and other neurological disorders [23]. The complex of glutamic acid and acetyl salicylic acid prepared by freeze-drying technique can be used as a novel oral drug delivery system which can be safely administered orally [22]. The sodium salt forms of glutamic acid like monosodium glutamate (MSG) and its derivatives are used as food additives and flavor enhancers.

Glutamic acid helps in transporting potassium through the blood-brain barrier by providing necessary nutrients to metabolize sugar and fats [24]. Glutamic acid is found in high concentration in the brain and it is the only amino acid metabolized by the brain. In the mammalian central nervous system, Glutamate acts as a major excitatory neurotransmitter and helps in fast synaptic neurotransmission as well as to complex various physiological processes which include memory, learning, neuronal cell death and plasticity [16]. Glutamic acid has the largest world market among the amino acids. In the food and pharmaceutical industries, the thermal stability of glutamic acid is very important because of its possible degradation, which may eventually impact the product quality and safety [22].

In order to understand the thermal behavior of L-Glutamic acid, few studies were done earlier and these were limited to the $\beta$ polymorph of L-Glutamic acid. One study proposed that the dimerization occurs in the first decomposition step of $\beta$ L-Glutamic acid and results in the formation of a diketopiperazine [25]. Another study proposed that the decomposition occurs to form pyroglutamic acid (P) as an intermediate compound [26]. Han Wu et al. performed the isothermal studies of solid state L-Glutamic acid and proposed that the $\alpha$ polymorph transforms irreversibly to $\beta$ polymorph and a two-step reaction occurs in which pyroglutamic acid (P) is formed due to internal cyclization followed by polymerization to form polyglutamic acid (PGA) [1]. The following figure shows the thermogravimetric curves of $\alpha$ and $\beta$ polymorphs of L-Glutamic acid:

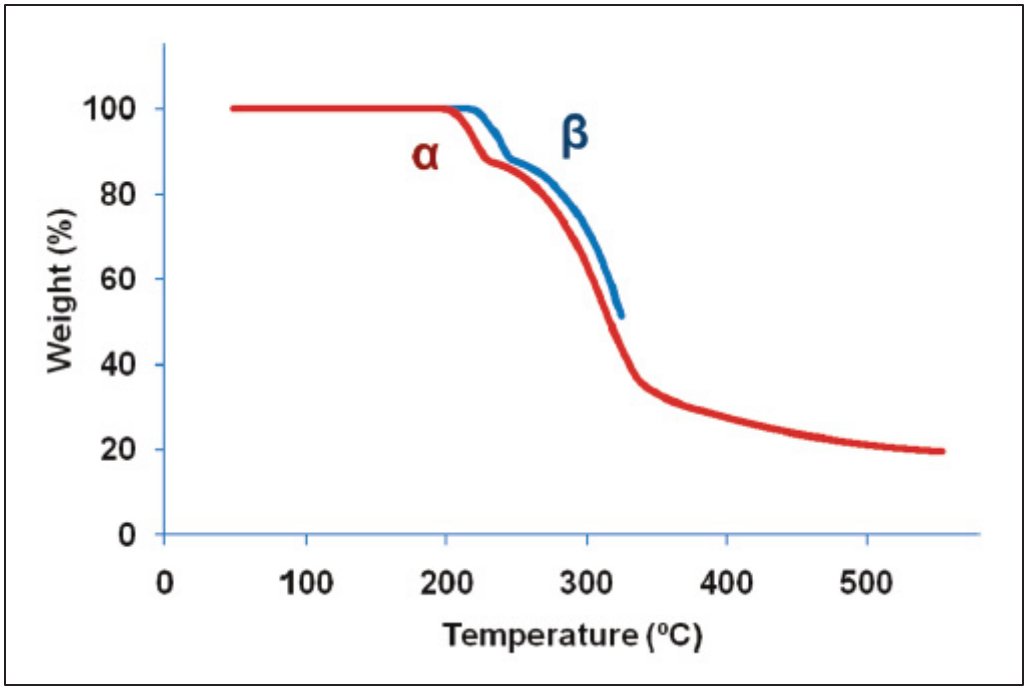


**Figure 2: Thermogravimetric curves of α and β polymorphs of L-Glutamic acid [1]**

The above figure shows that the weight loss in *β* polymorph occurs at a few degrees higher temperature when compared to that of *α* polymorph [1].

## Theory

In this study, the thermal analysis of aspartic acid and glutamic acid samples was performed using TGA and DSC instruments. The thermogravimetric experimental data were used to calculate the kinetic parameters like activation energy ($E_a$), pre-exponential factor ($A$) and order of the reaction ($n$) for the reactions occurring in each sample. The equations used to calculate the kinetics of thermal decomposition of the solid samples were derived as explained below.

### Determination of the $n^{th}$-order reaction kinetics [27]:

The information about the kinetics of thermal degradation processes can be obtained from thermogravimetry [48]. The general reaction rate equation for thermal decomposition of solids is given as:

$$\frac{\mathrm{d}\alpha}{\mathrm{d}t} = kf(\alpha) \qquad (1)$$

Where, $\alpha$ is the conversion fraction of solid sample

$t$ is the time elapsed for the reaction

$k$ is the rate constant for the reaction and

$f(\alpha)$ is the conversion function.

By assuming that the thermal decomposition of solids obeys $n^{th}$-order kinetics, the conversion function, $f(\alpha)$ in the above equation can be expressed as:

$$f(\alpha) = (1-\alpha)^n \qquad (2)$$

where, $n$ is the order of reaction and

$(1-\alpha)$ represents the portion of the sample that remains unreacted.

Thus, equation (1) can be written as:

$$\frac{\mathrm{d}\alpha}{\mathrm{d}t} = k(1-\alpha)^n \qquad (3)$$

The temperature dependence of chemical processes can be expressed in terms of Arrhenius equation, from which the reaction rate constant can be obtained experimentally. The Arrhenius equation is given as:

$$k = A\exp\left(-\frac{E_a}{RT}\right) \qquad (4)$$

where, $k$ is the reaction rate constant

$A$ is the pre-exponential factor

$E_a$ is the activation energy

$R$ is the ideal gas constant and

$T$ is the temperature.

Thus, the equation (3) can be further expanded as:

$$\frac{\mathrm{d}\alpha}{\mathrm{d}t} = k(1-\alpha)^n = A\exp\left(-\frac{E_a}{RT}\right)(1-\alpha)^n \qquad (5)$$

The conversion fraction $(\alpha)$ of the solid sample can be defined in terms of the fractional weight change of the sample, which is given as:

$$\alpha = \frac{w_0 - w}{w_0 - w_f} \qquad (6)$$

where, $w_0$, $w_f$ and $w$ are the initial weight, final weight and weight of the sample at time $t$, respectively.

The thermal reactions are usually carried out at a constant heating rate ($\beta$), which is therefore given as:

$$\beta = \frac{\mathrm{d}T}{\mathrm{d}t} \tag{7}$$

The equations (5) and (7) are combined, rearranged and integrated:

$$\int_0^{\alpha} \frac{\mathrm{d}\alpha}{(1-\alpha)^n} = \frac{1}{n-1}\left[\frac{1}{(1-\alpha)^{n-1}} - 1\right] = \frac{A}{\beta}\int_0^{T} \exp\left(-\frac{E_a}{RT}\right)\mathrm{d}T \tag{8}$$

The integral term on the right hand side of equation (8) is approximately solved by the Vyazovkin isoconversional method [28, 29]. Generally, for most of the applications, $\frac{E_a}{2RT} \gg 1$ which implies that $E_a$ is much greater than $2RT$. According to this method, from equation (8), the temperature integral can be approximated as shown:

$$\int_0^{T} \exp\left(-\frac{E_a}{RT}\right)\mathrm{d}T \approx \frac{RT^2}{E_a}\exp\left(-\frac{E_a}{RT}\right) \tag{9}$$

Substituting equation (9) in equation (8) gives:

$$\frac{1}{n-1}\left[\frac{1}{(1-\alpha)^{n-1}} - 1\right] = \frac{ART^2}{\beta E_a}\exp\left(-\frac{E_a}{RT}\right) = \frac{kRT^2}{\beta E_a} \tag{10}$$

As the temperature increases during a reaction, the rate of the reaction $\frac{\mathrm{d}\alpha}{\mathrm{d}t}$ will reach its maximum value and becomes zero as the reactant gets exhausted. Therefore,

differentiating equation (5) with respect to temperature or time equals zero when the rate of the reaction is maximum.

$$\frac{\mathrm{d}}{\mathrm{d}t}\left(\frac{\mathrm{d}\alpha}{\mathrm{d}t}\right) = \frac{\mathrm{d}\alpha}{\mathrm{d}t}\left[\frac{\beta}{RT^2} - An(1-\alpha)^{n-1}\exp\left(-\frac{E_a}{RT}\right)\right] = 0 \qquad (11)$$

Therefore, the equation (11) is solved as:

$$\frac{\beta E_a}{RT_m^2} = An(1-\alpha_m)^{n-1}\exp\left(-\frac{E_a}{RT_m}\right) = k_m n(1-\alpha_m)^{n-1} \qquad (12)$$

where, subscript *m* indicates the experimental parameter at the maximum reaction rate. The equations (10) and (12) are combined and rearranged to give:

$$1-\alpha_m = (1-\alpha)_m = n^{1/(1-n)} \qquad (13)$$

Therefore, from this equation, it is clear that the portion of sample that remains unreacted at a maximum reaction rate $(1-\alpha_m)$ and the order of reaction *n* are both related to each other. The term $(1-\alpha)_m$ can be found from TGA results and this can be used to determine *n* by using equation (13). Thus, when the thermal decomposition of solid is considered as an $n^{\text{th}}$-order reaction ($n \neq 1$), the value of *n* can be determined from thermogravimetric data.

Substituting equation (13) in equations (10) and (12) gives:

$$E_a = A\exp\left(-\frac{E_a}{RT_m}\right)\frac{RT_m^2}{\beta} = \frac{k_m RT_m^2}{\beta} \qquad (14)$$

Using the equations (5) and (13), the activation energy in equation (14) can be given as:

$$E_a = RT_m^2 (1-\alpha)_m^{-n} \left(\frac{\mathrm{d}\alpha}{\mathrm{d}T}\right)_m = n^{n/(n-1)} RT_m^2 \left(\frac{\mathrm{d}\alpha}{\mathrm{d}T}\right)_m \quad (15)$$

Then, the pre-exponential factor can be calculated as:

$$A = n^{n/(n-1)} \beta \left(\frac{d\alpha}{dT}\right)_m exp\left[n^{n/(n-1)} T_m \left(\frac{d\alpha}{dT}\right)_m\right] \quad (16)$$

Therefore, from the thermogravimetric data at a maximum reaction rate, using the information like reaction temperature and reaction rate, the kinetic parameters like activation energy and pre-exponential factor can be calculated.

**Determination of the first-order reaction kinetics [27]:**

When the thermal decomposition of a solid sample is considered as a simple first order reaction ($n$ = 1), the equation (5) can be written as:

$$\frac{\mathrm{d}\alpha}{\mathrm{d}t} = k(1-\alpha) = A \exp\left(-\frac{E_a}{RT}\right)(1-\alpha) \quad (17)$$

The equations (7) and (17) are combined, rearranged and integrated:

$$\int_0^\alpha \frac{\mathrm{d}\alpha}{(1-\alpha)} = \frac{A}{\beta}\int_0^T \exp\left(-\frac{E_a}{RT}\right)\mathrm{d}T \quad (18)$$

Substituting equation (9) in equation (18) and taking the logarithm gives:

$$-\ln(1-\alpha) = \frac{ART^2}{\beta E_a} \exp\left(-\frac{E_a}{RT}\right) = \frac{kRT^2}{\beta E_a} \quad (19)$$

As the temperature increases during a reaction, the rate of the reaction $\frac{\mathrm{d}\alpha}{\mathrm{d}t}$ will reach its maximum value and becomes zero as the reactant gets exhausted. Therefore,

differentiating equation (17) with respect to temperature or time equals zero when the rate of the reaction is maximum.

$$\frac{\mathrm{d}}{\mathrm{d}t}\left(\frac{\mathrm{d}\alpha}{\mathrm{d}t}\right) = \frac{\mathrm{d}\alpha}{\mathrm{d}t}\left[\frac{\beta}{RT^2} - A(1-\alpha)\exp\left(-\frac{E_a}{RT}\right)\right] = 0 \qquad (20)$$

Therefore, the equation (20) is solved as:

$$\frac{\beta E_a}{RT_m^2} = A\exp\left(-\frac{E_a}{RT_m}\right) = k_m \qquad (21)$$

where, subscript *m* indicates the experimental parameter at the maximum reaction rate. The equation (21) can be rearranged to give an equation which is same as equation (14):

$$E_a = A\exp\left(-\frac{E_a}{RT_m}\right)\frac{RT_m^2}{\beta} = \frac{k_m RT_m^2}{\beta} \qquad (22)$$

The equation (22) can be rearranged as:

$$k_m = \frac{\beta E_a}{RT_m^2} \qquad (23)$$

The equations (19) and (23) are combined and rearranged to give:

$$1 - \alpha_m = (1-\alpha)_m = 1/e \approx 0.37 \qquad (24)$$

Therefore, for a first order reaction, the portion of sample that remains unreacted at a maximum reaction rate $(1-\alpha_m)$ which can be found from TGA results is closely equal to 1/*e*. In equation (19), the $k_m$ term can be substituted by equation (17) and after rearrangement, the activation energy can be given as:

$$E_a = \frac{-RT_m^2}{(1-\alpha)_m \ln(1-\alpha)_m}\left(\frac{d\alpha}{dT}\right)_m = eRT_m^2\left(\frac{d\alpha}{dT}\right)_m \quad (25)$$

Then, the pre-exponential factor can be calculated as:

$$A = e\beta\left(\frac{d\alpha}{dT}\right)_m \exp\left[eT_m\left(\frac{d\alpha}{dT}\right)_m\right] \quad (26)$$

Therefore, from the thermogravimetric data at a maximum reaction rate, using the information like reaction temperature and reaction rate, the kinetic parameters of first order reactions can be calculated.

**Determination of the order of reaction, *n* [27]:**

As already mentioned, from the TGA data, the order of the reaction (*n*) can be determined using equation (13), which gives the relationship between the portion of sample that remains unreacted at a maximum reaction rate $(1-\alpha)_m$ and *n* (for $n \neq 1$). If $(1-\alpha)_m$ is equal or close to $1/e$, the reaction obeys the first order ($n = 1$). Thus, $1/e$ is the limit of equation (13) when $n \to 1$, which is given as:

$$\lim_{n\to 1} n^{1/(1-n)} = 1/e \quad (27)$$

By using equation (13), the order of the reaction, *n* is 1, 2, 3, 4 or 5 when $(1-\alpha)_m$ is 0.37, 0.50, 0.58, 0.63, or 0.67 respectively. When *n* is not an integer as mentioned above, its value is determined using an exponential regression equation, which is given as:

$$n = 0.1368 \exp[5.3635(1-\alpha)_m] \quad (28)$$

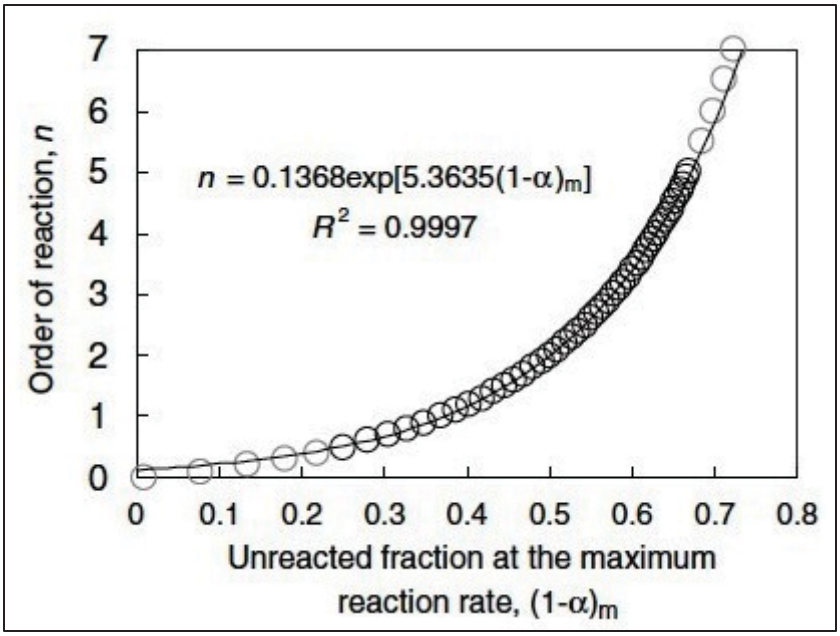


**Figure 3: Regressive relationship between the unreacted fraction of sample at the maximum reaction rate $(1-\alpha)_m$ and the order of reaction ($n$) [27]**

The above figure gives the regressive relationship between the unreacted fraction of sample at the maximum reaction rate $(1-\alpha)_m$ and the order of reaction $n$. For $(1-\alpha)_m$ between 0.25 and 0.67 (that is, $n$ between 0.5 and 5), the regression result [27] is very satisfactory, as shown in the figure [27]. Therefore, most of the reactions will be satisfied by equation (28). The regression in equation (28) cannot fit the relationship shown in equation (13), if $(1-\alpha)_m$ is greater than 0.77 (that is, $n > 10$). Therefore, the equation (28) cannot satisfy the reactions whose $n$ value is greater than 10 [27].

## Instrumentation

Thermal analysis (TA) includes a group of techniques in which the substance is subjected to a controlled temperature program and a physical property of the substance and/or its reaction products is measured as a function of temperature [30]. The definition of thermal analysis given by the ICTAC (International Confederation for Thermal Analysis and Calorimetry) is, “Thermal Analysis is a group of techniques that study the properties of materials as they change with the temperature”. Practically, the properties like thermal capacity, enthalpy, changes in mass and the coefficient of heat expansion can be obtained from thermal analysis. In solid state chemistry, reactions in the solid state, phase diagrams, phase transitions and thermal degradation reactions can be studied by using thermal analysis [31].

There are several types of thermal methods which differ in the properties measured and the temperature programs. The advantage of thermal analysis techniques is that only small amounts of samples are required and this helps in the distribution of temperature uniformly and ensures high resolution. The low heating rates give higher accuracies and oxidation of the sample can be prevented by using an inert atmosphere. They have a wide range of applications on industrial products which include polymers, metals and alloys, clays and minerals, pharmaceuticals and so on for quality control and research [32]. The thermal analysis methods used in this study include thermogravimetric analysis (TGA) and differential scanning calorimetry (DSC).

## Thermogravimetric Analysis (TGA):

Thermogravimetric Analysis (TGA) is an analytical technique used to characterize the materials by measuring the amount and rate of weight change of a substance as a function of temperature or time in a controlled atmosphere. Primarily, these measurements are used to predict the thermal stability of materials at temperatures up to 1000 °C by determining their composition. With this analytical technique, the fraction of volatile components in a compound can be identified by measuring the changes in the sample weight. The measurement is usually carried out in air or in an inert atmosphere using gases such as Nitrogen, Helium or Argon [47]. The sample is subjected to a controlled temperature program and the change in weight is measured and recorded as a function of temperature. The temperature is most often programmed to increase linearly. Isothermal studies can also be performed when the weight changes of sample with time are required [33].

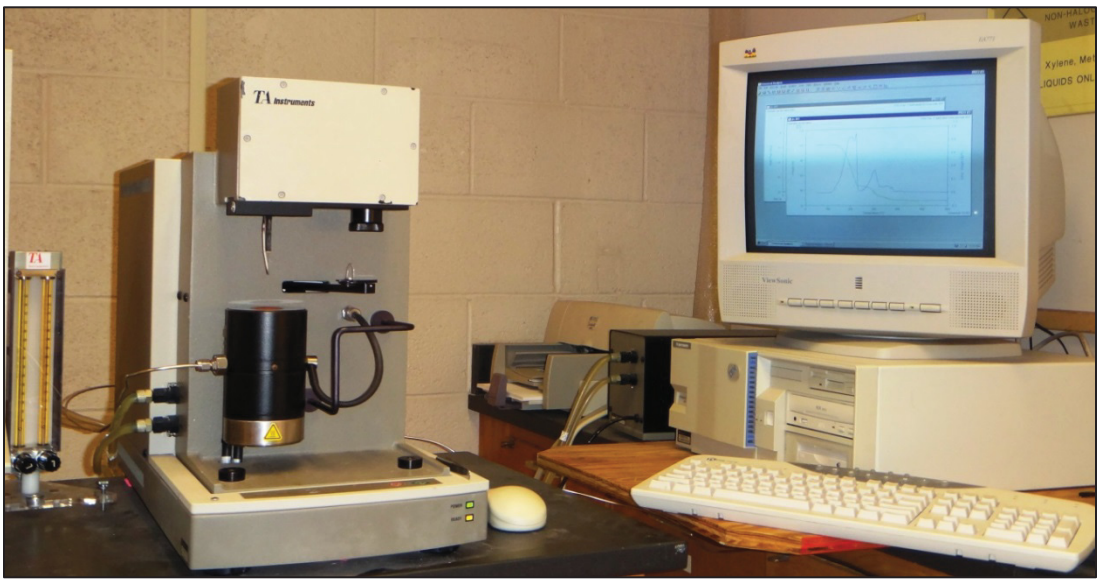


**Figure 4: TA Instruments – 2050 TGA interfaced with a computer**

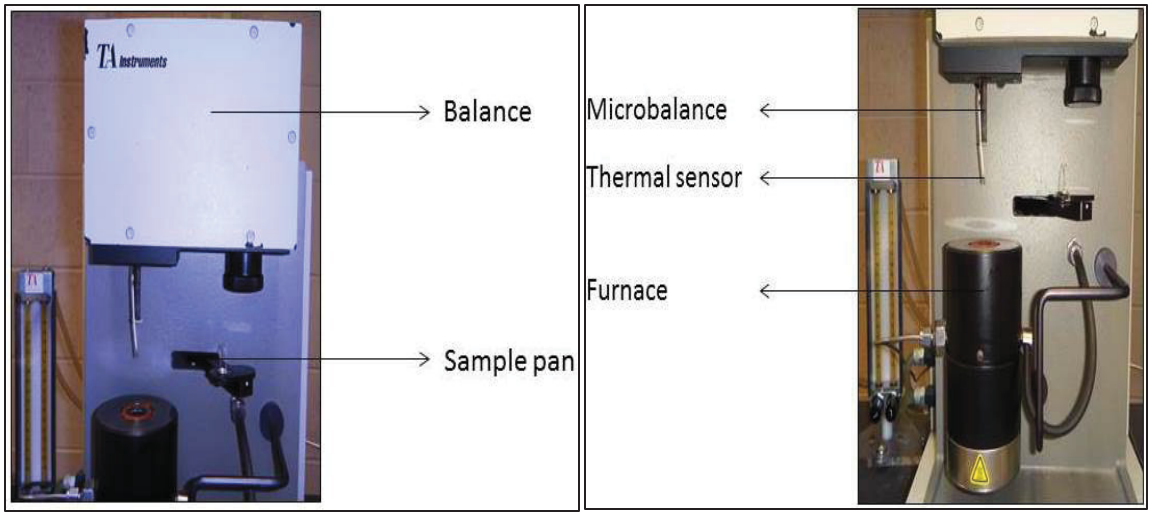


**Figure 5: Various components of TA 2050 TGA instrument**

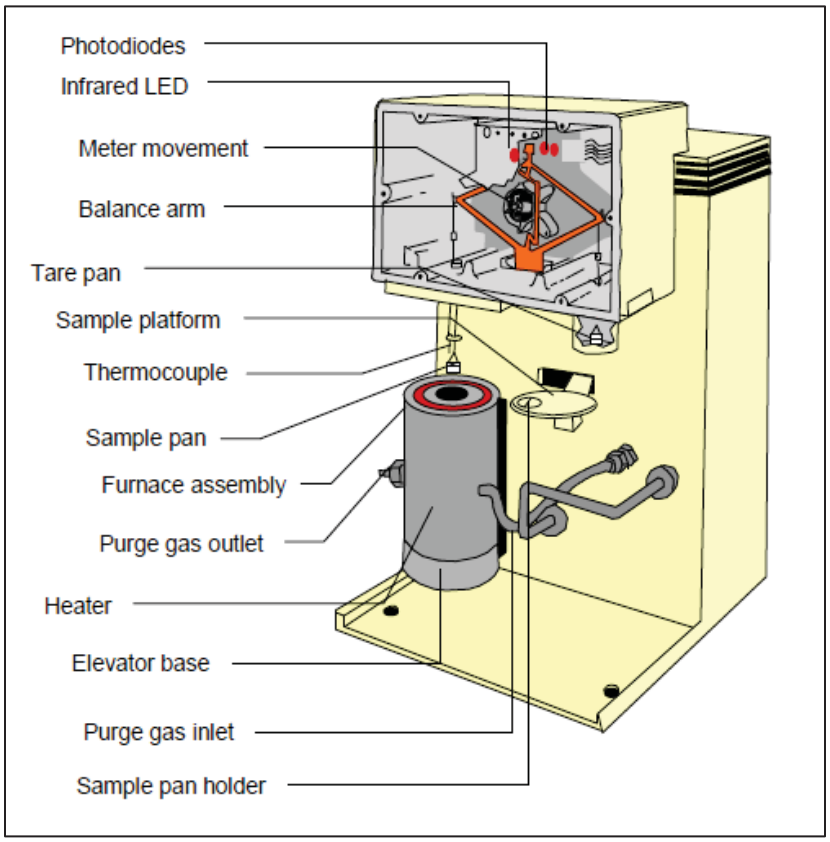


**Figure 6: Schematic diagram showing various components of TGA instrument [38]**

The TGA instrument consists of various essential components which include a thermobalance or microbalance, furnace, sample holder or pan, thermocouple and purge gas system. The sensitivity of the balance is usually around one microgram and the balance precision is up to 0.01 %. The capacity of the balance is a few hundred milligrams. The furnace is insulated and can withstand very high temperatures up to 1000 °C and the heating rates up to 100 °C per minute [34]. Sample pan is another important part of TGA instrument. The sample pans can be made of platinum, aluminum, alumina or ceramic pans with different sizes. The sample pan is selected based on the type of sample that needs to be analyzed [47]. Also, sample pan should be clean before loading the sample into it. Thermocouple acts as a temperature sensor which indicates the temperature of the sample and it is placed close to the sample. The purge gas system is an enclosure used for maintaining the required atmosphere. The controlled atmosphere is maintained by using inert gases like nitrogen, helium and argon or reactive gases like oxygen and hydrogen to mention a few. The TGA instrument is interfaced with a computer system for instrument control, temperature program, data collection, display and analysis [34].

The material or sample is heated by furnace under certain experimental conditions and the weight loss or weight gain occurs. This change in weight of the sample with increasing or decreasing temperature and with the time elapsed is recorded as a thermogram. The thermal stability of the samples, the kinetic parameters for the chemical reactions in the samples and the changes in the composition of samples can be determined from the measured weight loss curves. Thus, the shape of a TGA curve is dependent on the physico-chemical processes and kinetic events that occur over a specific

range of temperatures [35]. The reactions like oxidation and degradation which occur during a TGA experiment are dependent on the absolute temperature and the time elapsed at that temperature. Therefore, the shape of the curve and transition temperatures of the curve can be affected by any experimental parameter that alters the reaction rate. Some of these factors include the heating rate, size of the sample, particle size and packing of the sample, crucible shape, flow rate and nature of the gaseous atmosphere. These factors may alter the decomposition temperatures of the samples, resolution of the peaks and may even affect the progress of the reaction. Sometimes, in a TGA thermogram, the noisy and erratic records can arise due to external vibrations, uneven gas flow and pressure pulses in the lab [36].

The correct weight loss curve or thermogram and reproducibility can be obtained by following correct experimental procedures. Sample preparation, choice of crucible and thermal program are some of the important factors to be considered for successful experimental practice. High purity raw materials should be used and sample should be finely powdered to achieve greater contact area and better equilibrium conditions [36]. Sample sizes should be maintained at a minimum on a milligram scale for better results. In order to permit the completeness of reactions, the time must be sufficiently long at any temperature [31]. By lowering the ramp rates, the possible time lag in the oven temperature and the sample temperature can be reduced. To obtain precise results in TGA experiments, the temperature and weight are the critical parameters. Therefore, careful calibration for temperature and weight should be done periodically according to the specifications given by the instrument manufacturer. Especially for kinetic studies, temperature calibration is important, which can be achieved by using curie-point

standards or drop-weight methods. Weight calibration should be done using known samples possessing standard weights [47].

In a TGA experiment, the evaporation of residual moisture or solvent may account for the weight loss at lower temperatures but at higher temperatures, various processes like decomposition, reduction, evaporation and desorption may account for the weight loss. In decomposition, the chemical bonds break apart and in evaporation, the volatiles are lost at elevated temperatures [37]. When reducing atmosphere is used, the sample interacts with reducing gases like hydrogen, ammonia and results in reduction. The weight gain processes like absorption, oxidation due to interaction of the sample with an oxidizing atmosphere may also be measured with TGA. By identifying where the actual weight loss is started and also the inflection point on the TGA curve, a sample can be analyzed. At inflection point, the highest rate of weight loss can be identified and is called as the first derivative peak temperature. The parameters typically of interest are degradation onset temperature, initial weight ($w_i$), final weight ($w_f$), percent mass loss and energy of activation. The percent mass loss can be given as [38]:

$$\text{Percent mass loss} = 100(w_i - w_f)/w_i$$

TGA has a wide range of applications in research, testing and several fields of science and technology, as the quantitative data for any class of materials can be generated from TGA. It is applied in different areas like characterization of materials, determination of the moisture content and level of organic and inorganic components of many substances. It is used in thermal stability studies to determine the decomposition mechanisms and degradation temperatures. It is useful in corrosion studies by examining

the reaction of substances with reactive gases or vapors and to determine the decomposition points of solvent residues and explosives. In kinetic studies, TGA is used to analyze the kinetic parameters of weight loss or gain and also in simulating industrial processes [39, 48].

**Differential Scanning Calorimetry (DSC):**

Differential scanning calorimetry is the most widely used thermo-analytical technique to measure the difference in the heat flow to a sample and reference as a function of time and temperature [40]. In DSC, the sample and reference cells are subjected to a controlled increasing or decreasing temperature program. Though, the two cells are provided with constant energy, the temperature of sample cell lags behind when compared to the reference cell due to the thermal transitions that occur in the sample. Therefore, excess heat is required by the sample cell to maintain the same temperature as that of the reference cell. This difference in the heat energy uptake between the two cells is used to calculate the excess heat capacity, which gives information about the thermally induced processes in the sample. DSC is the thermal analysis method used in studying various thermal transitions which include solid-liquid, solid-solid and several other transitions as well as reactions. The thermal transition temperatures like melting temperatures of various kinds of samples in their solid, solution or mixed phases can also be determined by DSC [41].

(A)

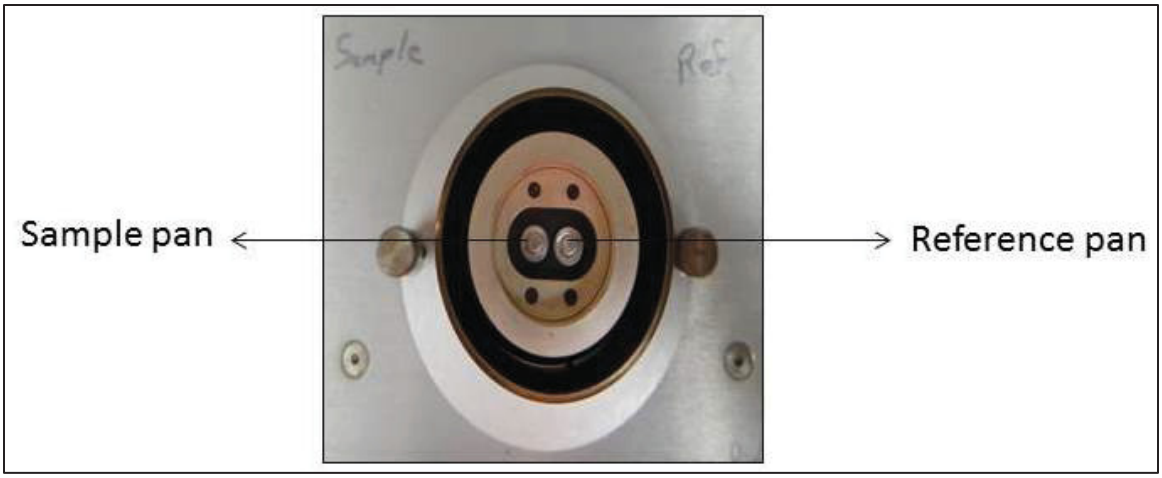


(B)

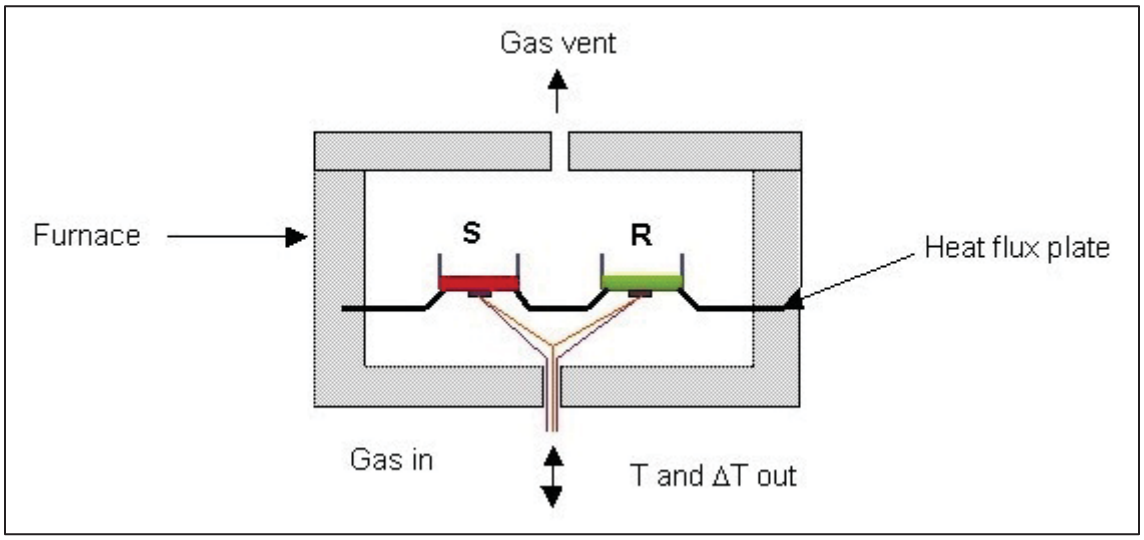


**Figure 7: DSC cell with sample and reference pans – (A) Horizontal cross-sectional view and Vertical cross-sectional view (B) [48]**

S = Sample pan

R = Reference pan

T = Temperature

ΔT = Difference in temperature

The fundamental thermodynamic information for thermally induced transitions, reactivity and various processes involved can be obtained by using a sensitive DSC instrument and with careful experimental analysis [40]. The DSC instrument consists of various essential components which include a sample holder, furnace, temperature sensors and a purge gas system. The sample holder has two raised platforms to place the reference pan and the sample pan [48]. The sample to be analyzed is placed uniformly in the sample pan and usually an empty pan is used as the reference pan. Since the pans are made of different materials (aluminum, platinum, copper, gold, alumina), they are selected based on their thermal properties, their reactivity and catalytic behavior with the samples under study. The sample cell and reference cell are present in a furnace made of a highly thermal conductive material [33]. Thermocouples act as the temperature sensors to detect and record the differential temperatures between the sample and reference pans. A dry and inert atmosphere is maintained in the cell by flowing inert purge gases (nitrogen, helium or argon) at a constant flow rate through the cell. Reactive gases (hydrogen, carbon dioxide) may also be used based on the type of analysis required. The purge gases help in increasing the heat transfer and also remove the volatiles and waste products formed due to thermal reactions of the samples apart from maintaining the required atmosphere in the DSC cell. The DSC instrument is interfaced with a computer system to control the temperature program, heating rates, data collection, storage and analysis [47, 48]. The main characteristics of an ideal DSC instrument are that, it should be capable of measuring the temperature changes and differential heat flow between the sample cell and reference cell by maintaining the constant heat flow rates. It should produce accurate and reproducible values with stable baseline and less noise [42].

**Figure 8: TA Instruments – 2910 DSC**

In a DSC experiment, when a sample is heated from room temperature to its decomposition temperature, the output is given as a thermogram or DSC curve. The DSC curve may show endothermic and/or exothermic peaks. The endothermic peak is due to the heat flow into the sample, indicating the amount of energy absorbed by the sample and the exothermic peak is due to the heat flow out of the sample, indicating the amount of energy released by the sample [37]. When the sample absorbs or releases heat, the difference in the heat flow ($\Delta dH/dt$) between the sample and reference arises. In endothermic processes like phase transitions, dehydrations, reduction reactions and some decomposition reactions, $\Delta dH/dt$ is positive, as the heat flow to the sample is greater than that to the reference. Whereas, in exothermic processes like crystallization, oxidation reactions and some decomposition reactions, $\Delta dH/dt$ is negative. The difference in the heat flow can be used to determine the changes in heat capacity and specific heat capacities [40]. From the DSC curve, the information such as the temperature at which certain processes or reactions (for example, melting point and decomposition of the

sample) occur can be determined. The peak temperature of the curve indicates the temperature at which the maximum reaction rate occurs. The enthalpy (Kcal/mol) of the reaction can be determined from the area under the peak of the DSC curve [43]. To obtain precise results in DSC experiments, the temperature and energy are the critical parameters. Therefore, careful calibration for temperature and energy should be performed periodically according to the specifications recommended by the instrument manufacturer. The temperature calibration can be achieved by using standard substances with high purity and precisely known melting points. Energy calibration may be performed using standard metals like zinc, indium and so on possessing known heat capacities and known heats of fusion [44].

DSC plays an important role in thermodynamic analysis and has wide range of practical applications in materials research, food technology, cosmetics, pharmaceutical and several other industries. It is used in finding thermal stability, melting points or melting profiles, glass transitions, polymorphic transitions, crystallization temperature, percent crystallinity, effect of additives, polymer blends and protein denaturation. DSC is widely applied in pharmaceutical industry to study the purity and stability of drugs, thermal transitions in DNA based drugs, shelf life and potency of pharmaceuticals. It is employed in drug development, drug absorption, to study their pharmacological as well as pharmacokinetic behavior, for testing the active pharmaceutical ingredients and quality control of drug design by detecting the impurities which cause variations in the thermogram. It helps in developing the novel drug delivery systems [45, 48].

DSC is used to identify the unknown materials by determining the values of $T_m$ (melting temperature) and $T_g$ (glass transition temperature), and comparing the DSC

profiles with that of a known material [42]. Apart from thermodynamic stability studies, the kinetic stability studies can be performed with DSC. In food industry, the thermal events like melting, crystallization, oxidation, dehydration, polymorphism, denaturation and decomposition are monitored by using DSC. It is applied to characterize the energetics of structural transitions in biological macromolecules by measuring the heat capacity difference between the folded and unfolded states of proteins, to determine the conformational changes in proteins and thermal denaturation, to study the stability of nucleic acids and melting of duplex DNA. It can also provide information about DNA binding to protein, lipid-protein interaction and protein-ligand binding [43, 46]. It is used for polymer characterization and $T_g$ is used to identify the polymers. DSC is used to safely analyze the explosives, to measure the energy released by a very small amount of a sample and to determine their stability which is required for safely handling. In automotive industry, DSC is used to analyze the lubricants and to determine their stability at high temperatures and pressures [37].

# Experimental Section

## Materials:

The compounds used in this study are L-Aspartic acid (L-Asp), L-Glutamic acid (L-Glu) and Potassium Chloride (KCl). All the three compounds used were in white powdered crystalline solid form as purchased from Aldrich, Sigma and J. T. Baker. These compounds were stored under room temperature and were used without any further purification.

**Table 1: List of compounds used in the study**

| Compound | Chemical formula | Fractional weight (g/mol) | Purity (%) | Supplier |
|---|---|---|---|---|
| L-Aspartic acid | $C_4H_7NO_4$ | 133.1 | 98+ % | Aldrich |
| L-Glutamic acid | $C_5H_9NO_4$ | 147.1 | 99 % | Sigma |
| Potassium Chloride | KCl | 74.55 | 99.7 % | J. T. Baker |

## Sample Preparation:

The blends of a single amino acid with KCl were prepared by manually mixing the corresponding amino acid and KCl crystals. The composition of blends ranges from 100 % neat amino acid to 10 %. The blends were in 10 % (w/w) intervals in the following weight ratios (amino acid : KCl); 90:10, 80:20, 70:30, 60:40, 50:50, 40:60, 30:70, 20:80, 10:90. Similar compositions were prepared for both the amino acids L-Asp and L-Glu separately. The L-Asp and L-Glu samples were labeled as Asp10, Asp20, Asp30, Asp40, Asp50, Asp60, Asp70, Asp80, Asp90, Asp100, Glu10, Glu20, Glu30, Glu40, Glu50,

Glu60, Glu70, Glu80, Glu90, and Glu100; the associated number indicates the % (w/w) composition of amino acid present in the samples.

Each composition of amino acid and KCl blend was prepared by measuring the amino acid and KCl by weight. Then, they were mixed and ground manually in a porcelain mortar with a porcelain pestle. The mixtures were transferred to glass vials with tightly closed caps and stored in a desiccator, under room temperature. These samples were used to perform both TGA and DSC measurements.

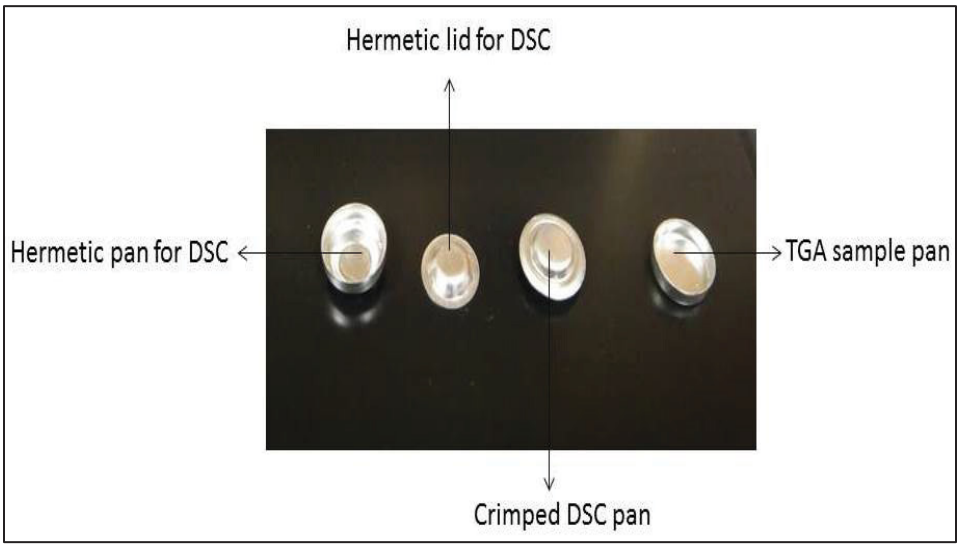


**Figure 9: Aluminum sample pans for DSC and TGA**

## Thermogravimetric Analysis:

The TGA measurements were carried out by using the instrument model 2050 TGA from TA Instruments. A sample of 14±0.35 mg was used for thermogravimetric analysis for all the sample compositions of both the amino acids L-Asp and L-Glu. The standard aluminum pans were used to hold the samples throughout the TGA experiments. The weight of empty pan was tared off initially and then the sample was weighed into

aluminum pan. All the TGA measurements were performed in Nitrogen atmosphere. The purge gas flow was set to 40 mL/min and the balance gas flow was set to 20 mL/min. Nitrogen was used as the purge gas as well as balance gas. The L-Asp samples of all compositions were equilibrated at 35 °C for 5 minutes and then heated to 600 °C at a ramp rate of 10 °C per minute. The L-Glu samples of all compositions were equilibrated at 35 °C for 5 minutes and then heated to 450 °C at a ramp rate of 10 °C per minute. The temperatures and the ramp rates were controlled by a computer program.

**Table 2: Experimental conditions for TGA**

| | |
|---|---|
| Instrument model | 2050 TGA |
| Sample weight | 14±0.35 mg |
| Purge gas | Nitrogen |
| Balance gas | Nitrogen |
| Purge gas flow rate | 40 mL/min |
| Balance gas flow rate | 20 mL/min |
| Ramp rate | 10 °C/min |
| Method for L-Asp samples | Ramp 10 °C/min up to 600 °C |
| Method for L-Glu samples | Ramp 10 °C/min up to 450 °C |

For each sample of L-Asp and L-Glu, three separate TGA runs were conducted with same experimental conditions so that the results can be cross-compared. The sample weight was maintained close for the three runs in order to obtain reproducibility. The TGA data was plotted as a thermogram with temperature (°C) on x-axis and weight % on

y-axis. Thus, the TGA scans were obtained for all the samples of Aspartic acid and Glutamic acid, after running them in TGA instrument as per the given experimental procedure. The TGA plots were analyzed by 'Universal Analysis', the software provided by TA Instruments. Using the same software, the three TGA scans obtained for each sample were converted to the text files format containing parameters like time, temperature and sample weight. This information from text files was further analyzed by PSI Plot version 9.5 (a software package from Poly Software International, Inc.). Each sample has three text files and the data points available in the text files were copied on to a PSI spreadsheet. The average values of each mentioned parameters were calculated on the PSI spreadsheet. The average temperature and the average sample weight columns were plotted on PSI plot with average temperature on x-axis and average sample weight on y-axis. From these plots, the values of initial weight of the sample ($w_i$) and the final weight, ($w_f$) at the inflection point of the first decomposition peak were obtained. Using these values, on the PSI spreadsheet, other variables like $\alpha$, $\frac{\mathrm{d}\alpha}{\mathrm{d}t}$ and temperature, T in kelvin (K) were calculated. The PSI plots were made with temperature, T (K) on x-axis and $\frac{\mathrm{d}\alpha}{\mathrm{d}t}$ ($^{\circ}C^{-1}$) on y-axis. From these plots, the variables like $\alpha_m$, $T_m$ and $\left(\frac{\mathrm{d}\alpha}{\mathrm{d}t}\right)_m$ were determined, which correspond to the values at the peak maximum of the peaks of all the samples of Aspartic acid and Glutamic acid.

The $\alpha_m$, $T_m$ and $\left(\frac{\mathrm{d}\alpha}{\mathrm{d}t}\right)_m$ values thus obtained were substituted in the equations given in the theory in order to calculate the kinetic parameters like activation energy ($E_a$), pre-exponential factor ($A$) and order of the reaction ($n$) for the reactions occurring in each sample.

The ball and stick molecular models of the biomolecules, amino acid - metal ion complexes and organic compounds were drawn using the software ChemDraw Ultra version 12.0 and ChemBioDraw3D Ultra version 12.0 from Cambridge Software Corporation.

## Fast Fourier Transform (FFT) Filter Smoothing:

The PSI plots with temperature, T (K) on x-axis and $\frac{d\alpha}{dt}$ ($°C^{-1}$) on y-axis have numerous scattered data points making it difficult to identify the accurate values of $\alpha_m$, $T_m$ and $\left(\frac{d\alpha}{dt}\right)_m$. To overcome this, the randomly scattered data points were eliminated and smooth curves were obtained in PSI plots by using Fast Fourier Transform (FFT) filter smoothing method in MATLAB software.

Fast Fourier Transform (FFT) filter smoothing is accomplished by removing Fourier components with frequencies higher than a cutoff frequency of:

$$F_{cutoff} = \frac{1}{n\Delta t}$$

where, *n* is the number of data points specified by the user, and Δt is the time (or more generally, the abscissa) spacing between two adjacent data points. Larger values of *n* result in lower cutoff frequencies, and thus a greater degree of smoothing. The function used to clip out the high-frequency components is a parabola with a maximum of 1 at zero frequency, and falling off to zero at the cutoff frequency defined above.

The filter smoothing of the PSI plots of aspartic acid samples was done by '10 FFT' method and for the PSI plots of glutamic acid samples, the filter smoothing was achieved by '5 FFT' method.

**Differential Scanning Calorimeter:**

The DSC measurements were carried out by using the instrument model 2910 DSC from TA Instruments. A sample of 10±0.60 mg was used for all the sample compositions of both the amino acids L-Asp and L-Glu. The hermetic aluminum pans with hermetic lids were used to load the samples throughout the DSC experiments. The weight of empty pan along with lid was tared and the sample was loaded and weighed. The weight of the samples was measured by using the balance in TGA instrument. Then, the pan was closed with lid and sealed. Empty hermetic aluminum pan sealed with hermetic lid was used as a reference pan for all the DSC experiments. The sample pan and reference pan were placed in the heating cell chamber of DSC instrument and it was closed with a glass cylinder. Nitrogen gas is purged through the instrument at a rate of 60 mL/min. The samples of all compositions of both the amino acids L-Asp and L-Glu were equilibrated at 35 °C for 5 minutes and then heated to 450 °C at a ramp rate of 10 °C per minute. The temperatures and the ramp rates were controlled by a computer program.

**Table 3: Experimental conditions for DSC**

| | |
|---|---|
| Instrument model | 2910 DSC |
| Sample weight | 10±0.60 mg |
| Purge gas | Nitrogen |
| Purge gas flow rate | 60 mL/min |
| Ramp rate | 10 °C/min |
| Method for L-Asp samples | Ramp 10 °C/min up to 450 °C |
| Method for L-Glu samples | Ramp 10 °C/min up to 450 °C |

All the DSC scans were made under the same experimental conditions. The DSC data was plotted as a thermogram with temperature (°C) on x-axis and heat flow (W/g) on y-axis. The TGA plots were analyzed by 'Universal Analysis', the software provided by TA Instruments.

# Results

## Thermogravimetric Analysis:

### Aspartic acid:

The $\alpha_m$, $T_m$ and $\left(\frac{d\alpha}{dt}\right)_m$ values obtained from the PSI plots with temperature, T (K) on x-axis and $\frac{d\alpha}{dt}$ (°C$^{-1}$) on y-axis for all the ten samples of Aspartic acid are shown in the table below:

**Table 4: Thermogravimetric experimental data of Aspartic acid samples**

| Sample | $w_i$ (mg) | $w_f$ (mg) | $T_m$ (K) | | $\alpha_m$ | | $\left(\frac{d\alpha}{dt}\right)_m$ (K$^{-1}$) | |
|---|---|---|---|---|---|---|---|---|
| | | | Peak1 | Peak2 | Peak1 | Peak2 | Peak1 | Peak2 |
| **Asp10** | 14.08 | 13.67 | 504.4 | 522.3 | 0.215 | 0.783 | 0.029 | 0.041 |
| **Asp20** | 14.11 | 13.18 | 505.3 | 523.6 | 0.228 | 0.755 | 0.026 | 0.039 |
| **Asp30** | 14.17 | 12.93 | 505.2 | 525.1 | 0.206 | 0.756 | 0.024 | 0.037 |
| **Asp40** | 14.08 | 12.58 | 505.8 | 525.1 | 0.219 | 0.732 | 0.023 | 0.036 |
| **Asp50** | 14.21 | 11.86 | 506.2 | 527.9 | 0.202 | 0.739 | 0.021 | 0.033 |
| **Asp60** | 14.07 | 11.52 | 506.8 | 528.1 | 0.208 | 0.726 | 0.020 | 0.033 |
| **Asp70** | 14.13 | 11.32 | 506.6 | 528.5 | 0.206 | 0.746 | 0.020 | 0.034 |
| **Asp80** | 14.16 | 11.00 | 507.8 | 529.4 | 0.224 | 0.751 | 0.020 | 0.033 |
| **Asp90** | 14.09 | 10.61 | 508.1 | 530.0 | 0.223 | 0.746 | 0.020 | 0.032 |
| **Asp100** | 14.12 | 10.24 | 509.6 | 531.9 | 0.232 | 0.746 | 0.019 | 0.031 |

The $\alpha_m$, $T_m$ and $\left(\frac{d\alpha}{dt}\right)_m$ values obtained in the above table were substituted in the equations given in the theory in order to calculate the kinetic parameters like activation energy ($E_a$), pre-exponential factor ($A$) and order of the reaction ($n$) for each sample. The $E_a$ and $A$ values were calculated using equations (15) and (16) for the first order reaction kinetics and equations (25) and (26) for the $n^{th}$ – order reaction kinetics of each sample. The $n$ value for each sample was calculated by using the equation (28) given in the theory. The calculated values of kinetic parameters for all the samples of Aspartic acid are tabulated below:

**Table 5: Kinetic parameters of Aspartic acid samples calculated from the TGA data**

| Sample | First Order Kinetics | | | | *n* - value | | *n*th Order Kinetics | | | |
|---|---|---|---|---|---|---|---|---|---|---|
| | $E_a$ (kJ $mol^{-1}$) | | A ($min^{-1}$) | | | | $E_a$ (kJ $mol^{-1}$) | | A ($min^{-1}$) | |
| | Peak 1 | Peak 2 | Peak 1 | Peak 2 | Peak 1 | Peak 2 | Peak 1 | Peak 2 | Peak 1 | Peak 2 |
| **Asp10** | 167.3 | 253.4 | 2.81E+15 | 4.08E+23 | 9.2 | 0.4 | 744.2 | 177.4 | 6.76E+75 | 7.17E+15 |
| **Asp20** | 148.3 | 244.1 | 2.50E+13 | 4.02E+22 | 8.6 | 0.5 | 622.4 | 181.0 | 1.05E+63 | 1.53E+16 |
| **Asp30** | 139.0 | 229.4 | 2.57E+12 | 1.09E+21 | 9.7 | 0.5 | 642.3 | 169.6 | 1.30E+65 | 9.16E+14 |
| **Asp40** | 134.7 | 224.9 | 8.64E+11 | 3.90E+20 | 9.0 | 0.6 | 588.5 | 175.1 | 2.72E+59 | 3.32E+15 |
| **Asp50** | 119.3 | 209.1 | 1.91E+10 | 7.34E+18 | 9.9 | 0.6 | 561.8 | 160.4 | 4.15E+56 | 8.59E+13 |
| **Asp60** | 117.3 | 210.5 | 1.12E+10 | 1.00E+19 | 9.6 | 0.6 | 536.9 | 166.2 | 9.03E+53 | 3.26E+14 |
| **Asp70** | 117.7 | 212.8 | 1.27E+10 | 1.63E+19 | 9.7 | 0.5 | 544.0 | 160.8 | 5.31E+54 | 8.98E+13 |
| **Asp80** | 116.5 | 206.5 | 8.83E+09 | 3.51E+18 | 8.8 | 0.5 | 497.2 | 154.2 | 5.40E+49 | 1.79E+13 |
| **Asp90** | 113.8 | 205.1 | 4.39E+09 | 2.38E+18 | 8.8 | 0.5 | 488.6 | 154.9 | 6.38E+48 | 2.05E+13 |
| **Asp100** | 111.5 | 197.6 | 2.32E+09 | 3.54E+17 | 8.4 | 0.5 | 460.3 | 149.2 | 5.35E+45 | 4.70E+12 |

The average initial weight loss of each aspartic acid sample from the three TGA scans was calculated as shown in the following table:

**Table 6: Initial weight loss of Aspartic acid samples in TGA experiments**

| Sample | 1st run (%) | 2nd run (%) | 3rd run (%) | Average (%) |
|---|---|---|---|---|
| **Asp10** | 4.47 | 2.16 | 2.61 | 3.08 |
| **Asp20** | 6.26 | 6.87 | 6.81 | 6.65 |
| **Asp30** | 9.02 | 8.57 | 8.89 | 8.83 |
| **Asp40** | 10.63 | 10.88 | 10.46 | 10.66 |
| **Asp50** | 16.47 | 17.29 | 15.65 | 16.47 |
| **Asp60** | 19.33 | 17.06 | 17.03 | 17.81 |
| **Asp70** | 18.49 | 20.51 | 20.63 | 19.88 |
| **Asp80** | 22.34 | 22.32 | 22.76 | 22.47 |
| **Asp90** | 24.63 | 25.44 | 23.60 | 24.56 |
| **Asp100** | 26.75 | 26.75 | 26.87 | 26.79 |

The mole ratios of aspartic acid to KCl for all the Aspartic acid samples were calculated as shown in the following table:

**Table 7: Mole ratios (Asp : KCl) of Aspartic acid samples**

| Sample | $w_i$ (mg) | No. of moles of Asp (moles) | No. of moles of KCl (moles) | Mole ratio (Asp : KCl) |
|---|---|---|---|---|
| **Asp10** | 14.08 | 0.01 | 0.17 | 0.06 |
| **Asp20** | 14.11 | 0.02 | 0.15 | 0.14 |
| **Asp30** | 14.17 | 0.03 | 0.13 | 0.24 |
| **Asp40** | 14.08 | 0.04 | 0.11 | 0.37 |
| **Asp50** | 14.21 | 0.05 | 0.10 | 0.56 |
| **Asp60** | 14.07 | 0.06 | 0.08 | 0.84 |
| **Asp70** | 14.13 | 0.07 | 0.06 | 1.31 |
| **Asp80** | 14.16 | 0.09 | 0.04 | 2.24 |
| **Asp90** | 14.09 | 0.10 | 0.02 | 5.04 |
| **Asp100** | 14.12 | 0.11 | 0.00 | 10.00 |

The mole ratio of Asp100 was approximated to a value of 10.00 to be in line with the mole ratios of other samples, when plotted. The activation energies ($E_a$) obtained for both peak 1 and peak 2 of Aspartic acid samples were plotted against the mole ratios of those samples, for both first order and $n^{th}$ order kinetics. The resulting plots with mole ratio on x-axis and $E_a$ on y-axis were shown below:

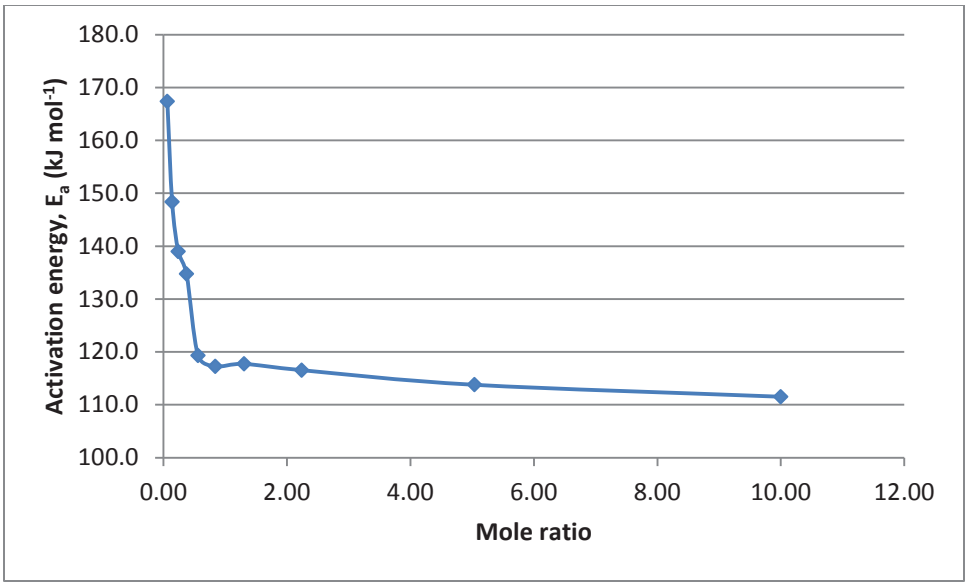


**Figure 10: Activation energies of first order reactions for peak 1 versus mole ratios of Aspartic acid samples**

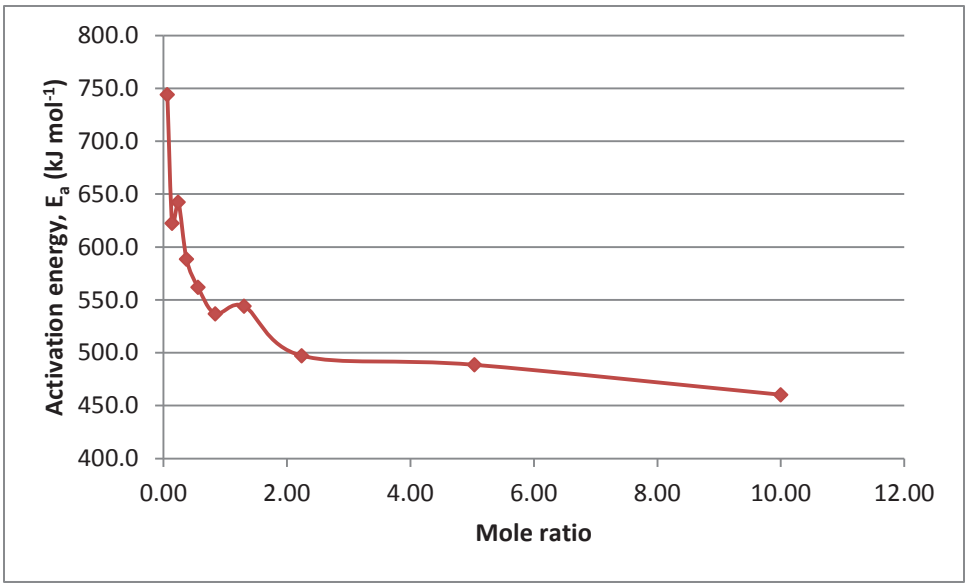


**Figure 11: Activation energies of $n^{th}$ order reactions for Peak 1 versus mole ratios of Aspartic acid samples**

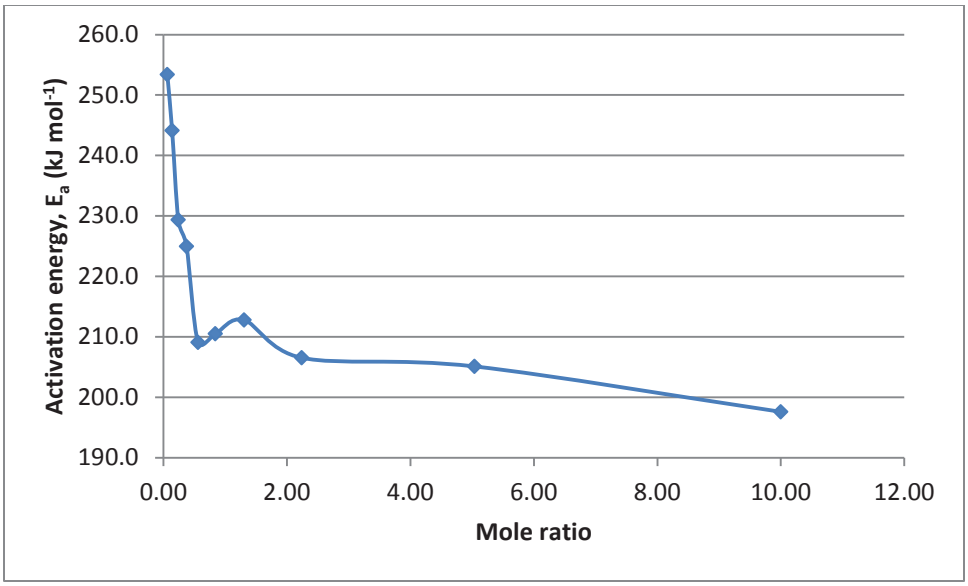


**Figure 12: Activation energies of first order reactions for peak 2 versus mole ratios of Aspartic acid samples**

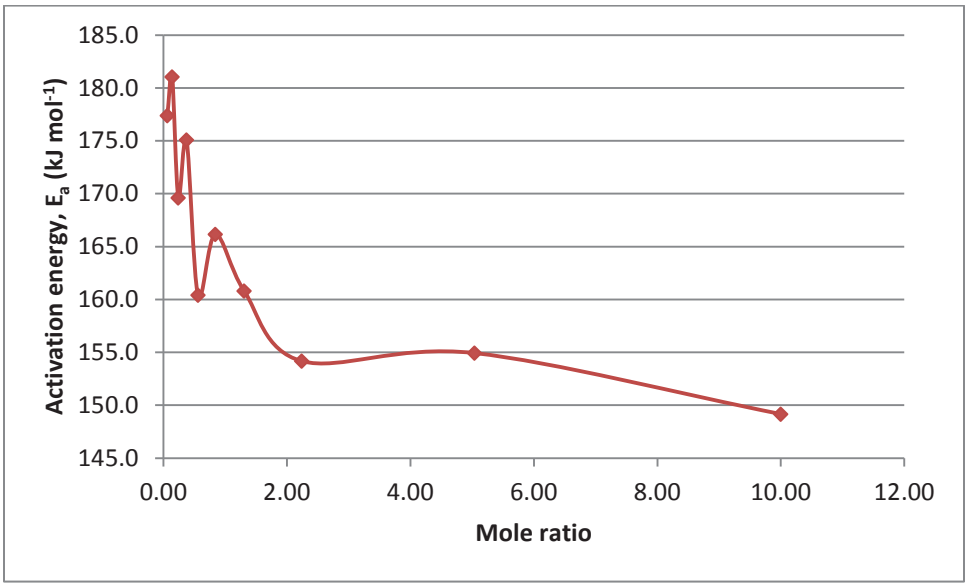


**Figure 13: Activation energies of $n^{th}$ order reactions for Peak 2 versus mole ratios of Aspartic acid samples**

**Aspartic acid (FFT):**

The PSI plots with temperature, T (K) on x-axis and $\frac{d\alpha}{dt}$ ($°C^{-1}$) on y-axis for all the samples of Aspartic acid were smoothened using 10 FFT method in the MATLAB software. The smoothened plots of all the samples of Aspartic acid were overlaid as shown in the following figure:

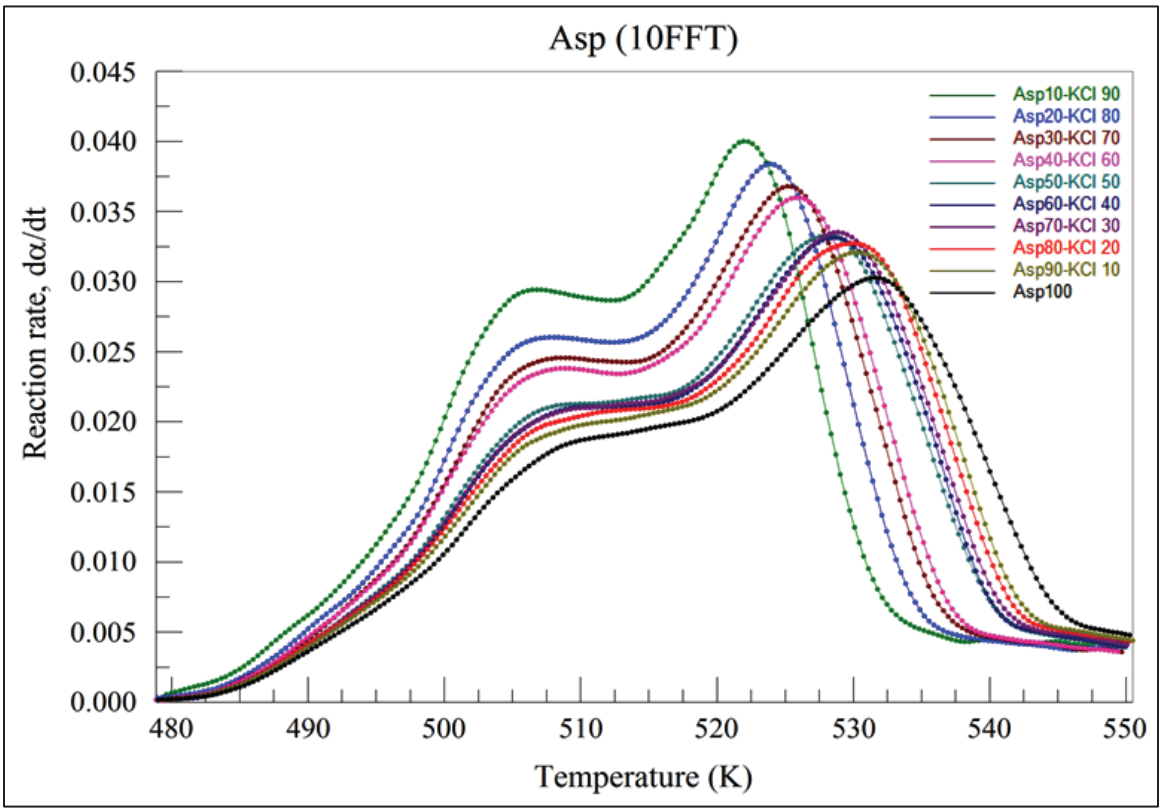


**Figure 14: Overlay of PSI plots of reaction rate profiles of Aspartic acid samples versus temperature**

From these plots, the variables like $T_m$ and $\left(\frac{d\alpha}{dt}\right)_m$ were determined, which correspond to the values at the peak maximum of the peaks of all the samples of Aspartic

acid. The $T_m$ and $\left(\frac{d\alpha}{dt}\right)_m$ values obtained for all the ten samples of Aspartic acid are tabulated below:

**Table 8: Thermogravimetric experimental parameters of Aspartic acid samples after FFT smoothing of PSI plots**

| Sample 10 FFT | $T_m$ (K) | | $\left(\frac{d\alpha}{dt}\right)_m$ ($K^{-1}$) | |
|---|---|---|---|---|
| | Peak1 | Peak2 | Peak1 | Peak2 |
| **Asp10** | 505.1 | 521.9 | 0.029 | 0.040 |
| **Asp20** | 505.7 | 523.6 | 0.026 | 0.038 |
| **Asp30** | 506.2 | 524.8 | 0.024 | 0.037 |
| **Asp40** | 506.5 | 525.4 | 0.023 | 0.036 |
| **Asp50** | 507.2 | 527.9 | 0.021 | 0.033 |
| **Asp60** | 507.8 | 528.4 | 0.021 | 0.033 |
| **Asp70** | 507.9 | 528.5 | 0.021 | 0.034 |
| **Asp80** | 508.4 | 529.4 | 0.020 | 0.033 |
| **Asp90** | 508.8 | 530.0 | 0.020 | 0.032 |
| **Asp100** | 509.6 | 531.2 | 0.019 | 0.030 |

The $T_m$ and $\left(\frac{d\alpha}{dt}\right)_m$ values obtained in the above table were substituted in the equations given in the theory in order to calculate the kinetic parameters like activation energy $(E_a)$, pre-exponential factor $(A)$ and order of the reaction $(n)$ for each sample. The $E_a$ and $A$ values were calculated using equations (15) and (16) for the first order reaction kinetics and equations (25) and (26) for the $n^{th}$ – order reaction kinetics of each sample. The $n$ value for each sample was calculated by using the equation (28) given in the theory. The calculated values of kinetic parameters for all the samples of Aspartic acid are shown in Table 9. The activation energies ($E_a$) obtained for both peak 1 and peak 2 of Aspartic acid samples were plotted against the mole ratios of those samples, for both first order and $n^{th}$ order kinetics, with the mole ratio on x-axis and $E_a$ on y-axis.

**Table 9: Kinetic parameters of Aspartic acid samples calculated from TGA data after FFT smoothing of PSI plots**

| Sample 10 FFT | First Order Kinetics | | | | *n* - value | | *n*th Order Kinetics | | | |
|---|---|---|---|---|---|---|---|---|---|---|
| | $E_a$ (kJ $mol^{-1}$) | | A ($min^{-1}$) | | | | $E_a$ (kJ $mol^{-1}$) | | A ($min^{-1}$) | |
| | Peak 1 | Peak 2 | Peak 1 | Peak 2 | Peak 1 | Peak 2 | Peak 1 | Peak 2 | Peak 1 | Peak 2 |
| **Asp10** | 166.6 | 246.3 | 2.24E+15 | 8.03E+22 | 9.2 | 0.4 | 741.1 | 172.4 | 2.52E+75 | 2.28E+15 |
| **Asp20** | 148.0 | 237.3 | 2.22E+13 | 8.17E+21 | 8.6 | 0.5 | 620.8 | 176.0 | 6.51E+62 | 4.65E+15 |
| **Asp30** | 139.0 | 228.4 | 2.38E+12 | 9.08E+20 | 9.7 | 0.5 | 642.2 | 168.9 | 9.31E+64 | 8.02E+14 |
| **Asp40** | 135.1 | 224.0 | 9.01E+11 | 3.01E+20 | 9.0 | 0.6 | 590.0 | 174.3 | 3.27E+59 | 2.71E+15 |
| **Asp50** | 121.5 | 209.7 | 3.09E+10 | 8.50E+18 | 9.9 | 0.6 | 572.3 | 160.9 | 3.86E+57 | 9.62E+13 |
| **Asp60** | 120.1 | 208.9 | 2.09E+10 | 6.65E+18 | 9.6 | 0.6 | 549.7 | 164.9 | 1.49E+55 | 2.35E+14 |
| **Asp70** | 120.1 | 211.5 | 2.10E+10 | 1.21E+19 | 9.7 | 0.5 | 555.0 | 159.8 | 5.15E+55 | 7.19E+13 |
| **Asp80** | 117.4 | 207.2 | 1.06E+10 | 4.06E+18 | 8.8 | 0.5 | 501.0 | 154.6 | 1.14E+50 | 2.00E+13 |
| **Asp90** | 114.1 | 203.8 | 4.55E+09 | 1.77E+18 | 8.8 | 0.5 | 489.9 | 154.0 | 7.45E+48 | 1.64E+13 |
| **Asp100** | 109.2 | 193.3 | 1.30E+09 | 1.38E+17 | 8.4 | 0.5 | 450.6 | 145.9 | 5.32E+44 | 2.30E+12 |

The resulting plots of all aspartic acid samples (FFT) were shown below:

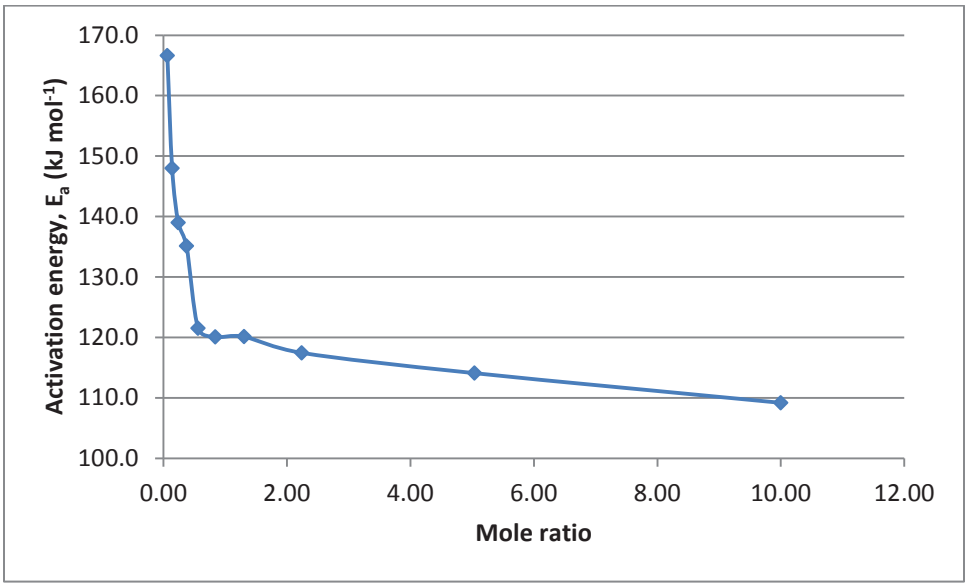


**Figure 15: Activation energies of first order reactions for peak 1 versus mole ratios of Aspartic acid samples after FFT smoothing of PSI plots**

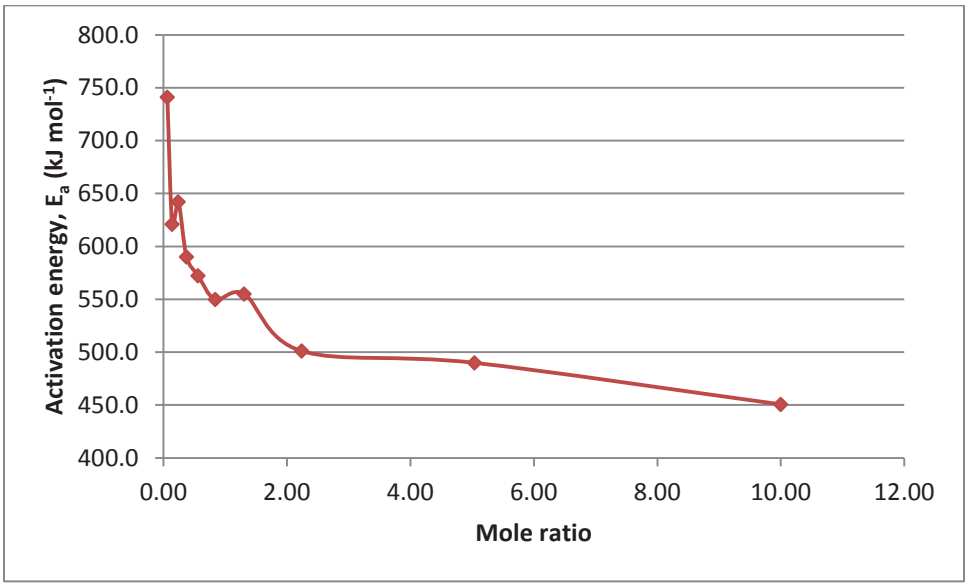


**Figure 16: Activation energies of $n^{th}$ order reactions for peak 1 versus mole ratios of Aspartic acid samples after FFT smoothing of PSI plots**

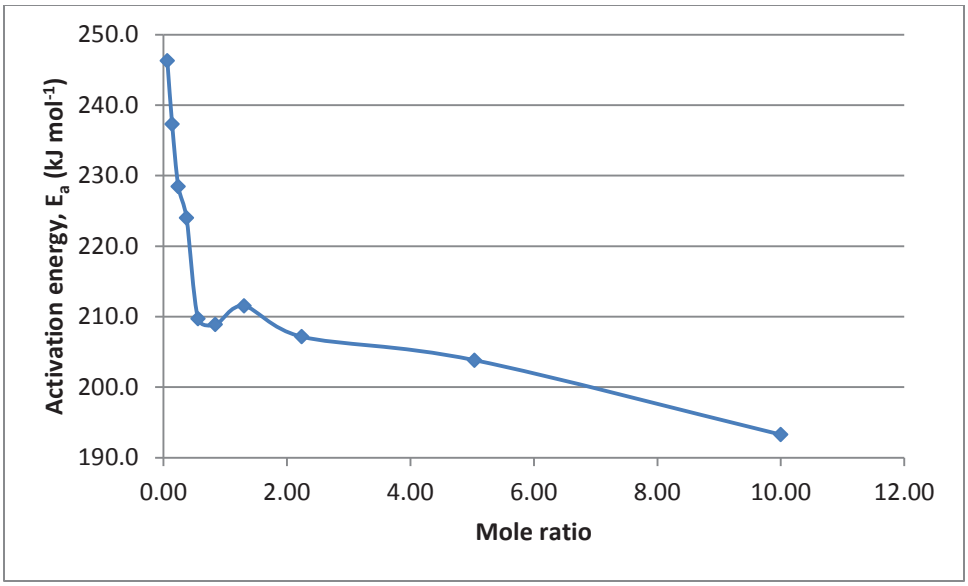


**Figure 17: Activation energies of first order reactions for peak 2 versus mole ratios of Aspartic acid samples after FFT smoothing of PSI plots**

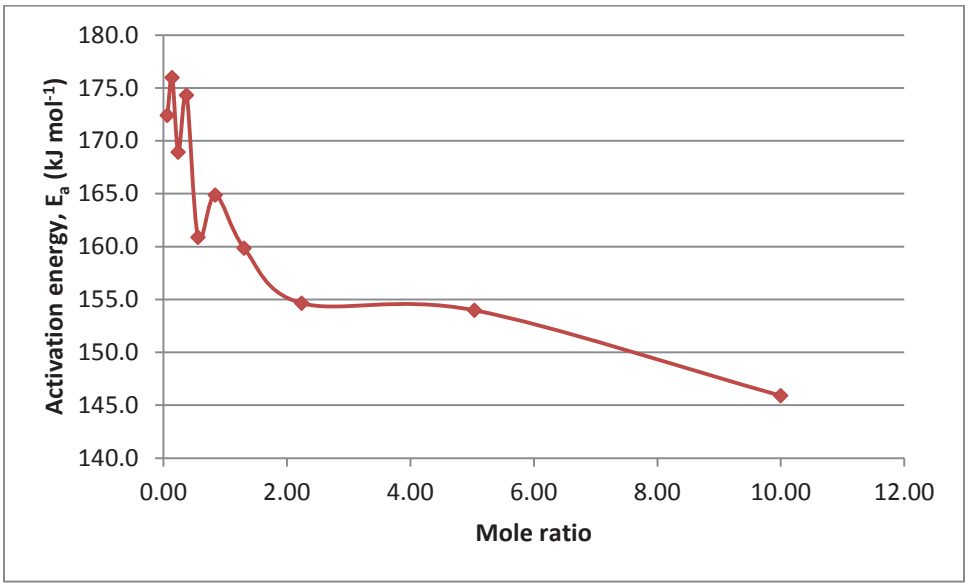


**Figure 18: Activation energies of $n^{th}$ order reactions for peak 2 versus mole ratios of Aspartic acid samples after FFT smoothing of PSI plots**

**Glutamic acid:**

The $\alpha_m$, $T_m$ and $\left(\frac{d\alpha}{dt}\right)_m$ values obtained from the PSI plots with temperature, T (K) on x-axis and $\frac{d\alpha}{dt}$ ($°C^{-1}$) on y-axis for all the ten samples of Glutamic acid are tabulated below:

**Table 10: Thermogravimetric experimental parameters of Glutamic acid samples**

| Sample | $w_i$ (mg) | $w_f$ (mg) | $T_m$ (K) | | $\alpha_m$ | | $\left(\frac{d\alpha}{dt}\right)_m$ ($K^{-1}$) | |
|---|---|---|---|---|---|---|---|---|
| | | | Peak1 | Peak2 | Peak1 | Peak2 | Peak1 | Peak2 |
| **Glu10** | 14.31 | 14.08 | 471.7 | - | 0.616 | - | 0.161 | - |
| **Glu20** | 14.11 | 13.73 | 472.1 | - | 0.621 | - | 0.150 | - |
| **Glu30** | 14.23 | 13.64 | 472.2 | 474.0 | 0.571 | 0.778 | 0.120 | 0.112 |
| **Glu40** | 14.21 | 13.52 | 471.6 | 474.3 | 0.501 | 0.803 | 0.113 | 0.123 |
| **Glu50** | 14.31 | 13.45 | 471.8 | 474.8 | 0.457 | 0.752 | 0.099 | 0.109 |
| **Glu60** | 14.05 | 13.08 | 472.0 | 475.0 | 0.458 | 0.734 | 0.094 | 0.111 |
| **Glu70** | 14.19 | 12.94 | 472.5 | 476.0 | 0.435 | 0.701 | 0.079 | 0.096 |
| **Glu80** | 14.20 | 12.86 | 472.8 | 476.9 | 0.438 | 0.748 | 0.078 | 0.093 |
| **Glu90** | 14.27 | 12.78 | 473.3 | 477.8 | 0.427 | 0.738 | 0.074 | 0.086 |
| **Glu100** | 14.35 | 12.74 | 474.4 | 479.0 | 0.485 | 0.783 | 0.074 | 0.081 |

The $\alpha_m$, $T_m$ and $\left(\frac{d\alpha}{dt}\right)_m$ values obtained in the above table were substituted in the equations given in the theory in order to calculate the kinetic parameters like activation energy ($E_a$), pre-exponential factor ($A$) and order of the reaction ($n$) for each sample. The $E_a$ and $A$ values were calculated using equations (15) and (16) for the first order reaction kinetics and equations (25) and (26) for the $n^{th}$ – order reaction kinetics of each sample. The $n$ value for each sample was calculated by using the equation (28) given in the theory. The calculated values of kinetic parameters for all the samples of Glutamic acid are tabulated below:

**Table 11: Kinetic parameters of Glutamic acid samples calculated from the TGA data**

| Sample | First Order Kinetics | | | | *n* - value | | *n*th Order Kinetics | | | |
|---|---|---|---|---|---|---|---|---|---|---|
| | $E_a$ (kJ $mol^{-1}$) | | A ($min^{-1}$) | | | | $E_a$ (kJ $mol^{-1}$) | | A ($min^{-1}$) | |
| | Peak 1 | Peak 2 | Peak 1 | Peak 2 | Peak 1 | Peak 2 | Peak 1 | Peak 2 | Peak 1 | Peak 2 |
| **Glu10** | 809.2 | - | 2.92E+88 | - | 1.1 | - | 839.4 | - | 6.75E+91 | - |
| **Glu20** | 754.5 | - | 2.06E+82 | - | 1.0 | - | 771.0 | - | 1.41E+84 | - |
| **Glu30** | 602.6 | 568.3 | 2.52E+65 | 2.12E+61 | 1.4 | 0.4 | 710.8 | 401.8 | 2.76E+77 | 6.75E+42 |
| **Glu40** | 567.9 | 625.4 | 4.12E+61 | 4.14E+67 | 2.0 | 0.4 | 834.0 | 421.1 | 1.80E+91 | 8.95E+44 |
| **Glu50** | 495.5 | 555.4 | 3.23E+53 | 6.21E+59 | 2.5 | 0.5 | 844.3 | 414.5 | 2.30E+92 | 1.47E+44 |
| **Glu60** | 471.3 | 564.1 | 6.06E+50 | 5.29E+60 | 2.5 | 0.6 | 799.7 | 436.8 | 2.29E+87 | 4.15E+46 |
| **Glu70** | 400.2 | 493.6 | 6.21E+42 | 6.42E+52 | 2.8 | 0.7 | 736.6 | 412.4 | 1.73E+80 | 6.60E+43 |
| **Glu80** | 392.6 | 477.5 | 8.23E+41 | 8.42E+50 | 2.8 | 0.5 | 715.3 | 359.0 | 6.79E+77 | 6.56E+37 |
| **Glu90** | 376.2 | 445.2 | 1.10E+40 | 1.84E+47 | 3.0 | 0.6 | 711.6 | 341.7 | 2.14E+77 | 6.83E+35 |
| **Glu100** | 374.9 | 420.0 | 6.32E+39 | 2.34E+44 | 2.2 | 0.4 | 578.9 | 294.0 | 2.80E+62 | 2.91E+30 |

The average initial weight loss of each glutamic acid sample from the three TGA scans was calculated as shown in the following table:

**Table 12: Initial weight loss of Glutamic acid samples in TGA experiments**

| Sample | 1st run (%) | 2nd run (%) | 3rd run (%) | Average (%) |
|---|---|---|---|---|
| **Glu10** | 2.06 | 1.49 | 1.77 | 1.77 |
| **Glu20** | 2.70 | 2.95 | 3.11 | 2.92 |
| **Glu30** | 4.26 | 4.06 | 4.09 | 4.14 |
| **Glu40** | 5.41 | 4.89 | 5.14 | 5.14 |
| **Glu50** | 6.45 | 6.26 | 6.35 | 6.35 |
| **Glu60** | 7.19 | 7.14 | 7.23 | 7.19 |
| **Glu70** | 8.47 | 8.98 | 8.34 | 8.59 |
| **Glu80** | 9.55 | 9.51 | 9.59 | 9.55 |
| **Glu90** | 10.34 | 10.31 | 10.30 | 10.32 |
| **Glu100** | 11.56 | 11.67 | 11.72 | 11.65 |

The mole ratios of glutamic acid to KCl for all the glutamic acid samples were calculated as shown in the following table:

**Table 13: Mole ratios (Glu : KCl) of Glutamic acid samples**

| Sample | $w_i$ (mg) | No. of moles of Glu (moles) | No. of moles of KCl (moles) | Mole ratio (Glu : KCl) |
|---|---|---|---|---|
| **Glu10** | 14.31 | 0.01 | 0.17 | 0.06 |
| **Glu20** | 14.11 | 0.02 | 0.15 | 0.13 |
| **Glu30** | 14.23 | 0.03 | 0.13 | 0.22 |
| **Glu40** | 14.21 | 0.04 | 0.11 | 0.34 |
| **Glu50** | 14.31 | 0.05 | 0.10 | 0.51 |
| **Glu60** | 14.05 | 0.06 | 0.08 | 0.76 |
| **Glu70** | 14.19 | 0.07 | 0.06 | 1.18 |
| **Glu80** | 14.20 | 0.08 | 0.04 | 2.03 |
| **Glu90** | 14.27 | 0.09 | 0.02 | 4.56 |
| **Glu100** | 14.35 | 0.10 | 0.00 | 10.00 |

The mole ratio of Glu100 was approximated to a value of 10.00 to be in line with the mole ratios of other samples, when plotted. The activation energies ($E_a$) obtained for both peak 1 and peak 2 of Glutamic acid samples were plotted against the mole ratios of those samples, for both first order and $n^{th}$ order kinetics. The resulting plots with mole ratio on x-axis and $E_a$ on y-axis were shown below:

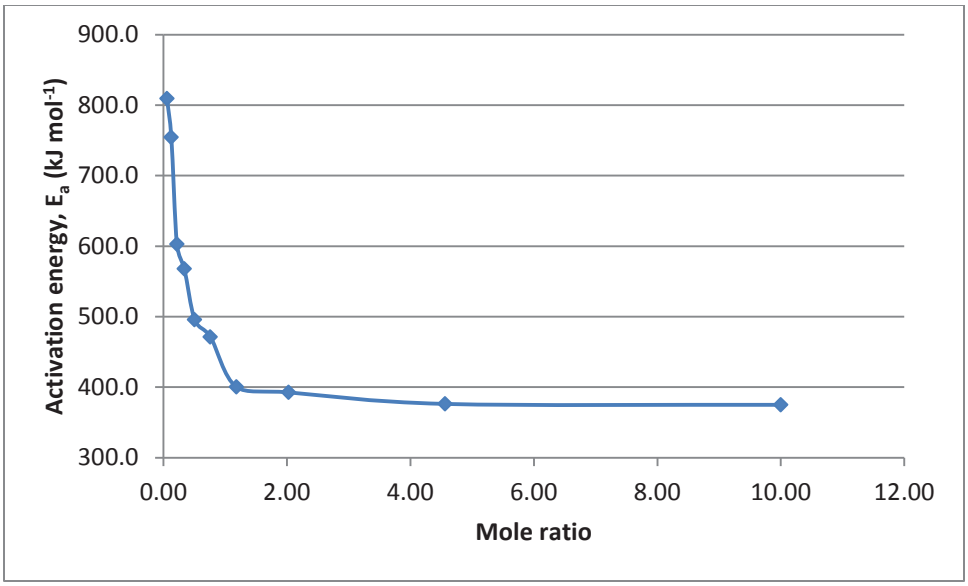


**Figure 19: Activation energies of first order reactions for peak 1 versus mole ratios of Glutamic acid samples**

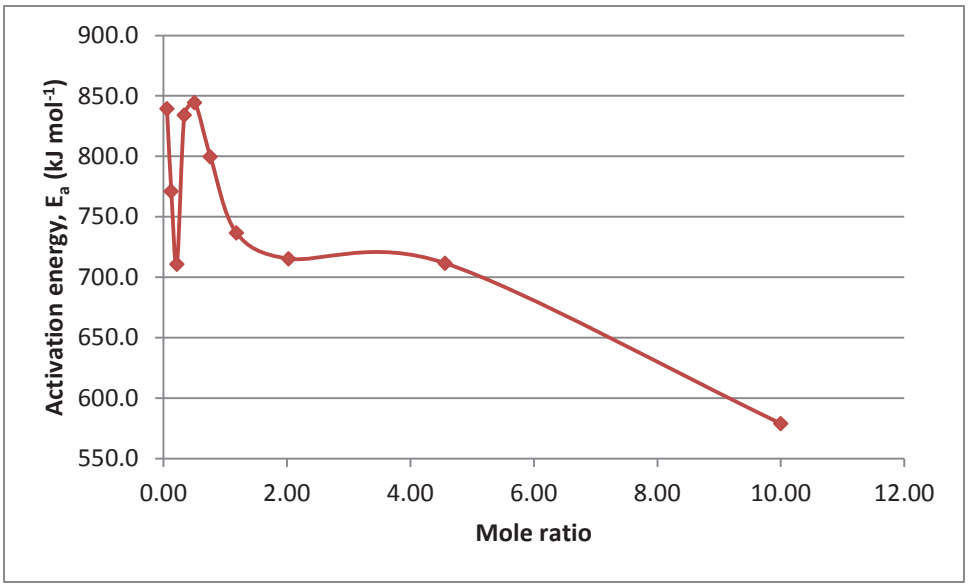


**Figure 20: Activation energies of $n^{th}$ order reactions for peak 1 versus mole ratios of Glutamic acid samples**

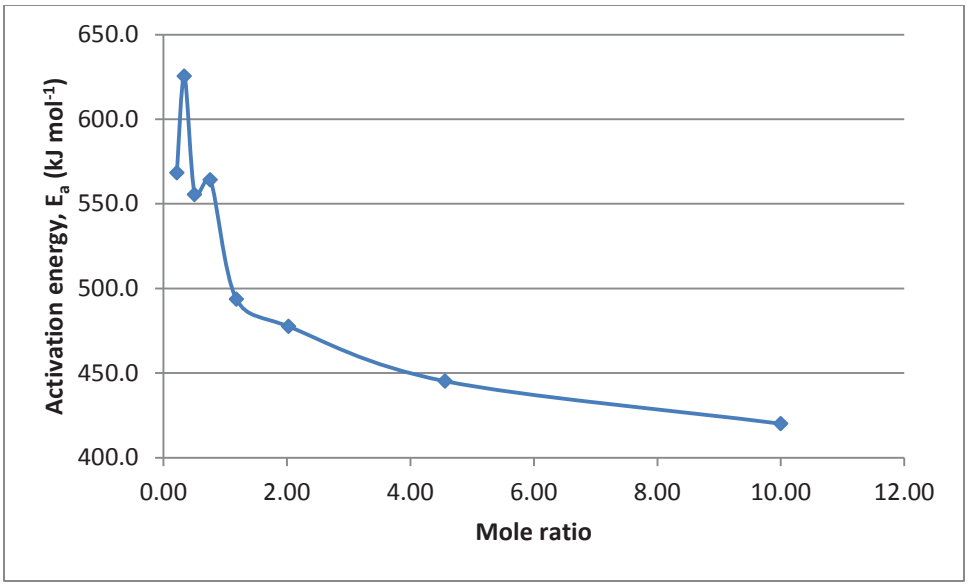


**Figure 21: Activation energies of first order reactions for peak 2 versus mole ratios of Glutamic acid samples**

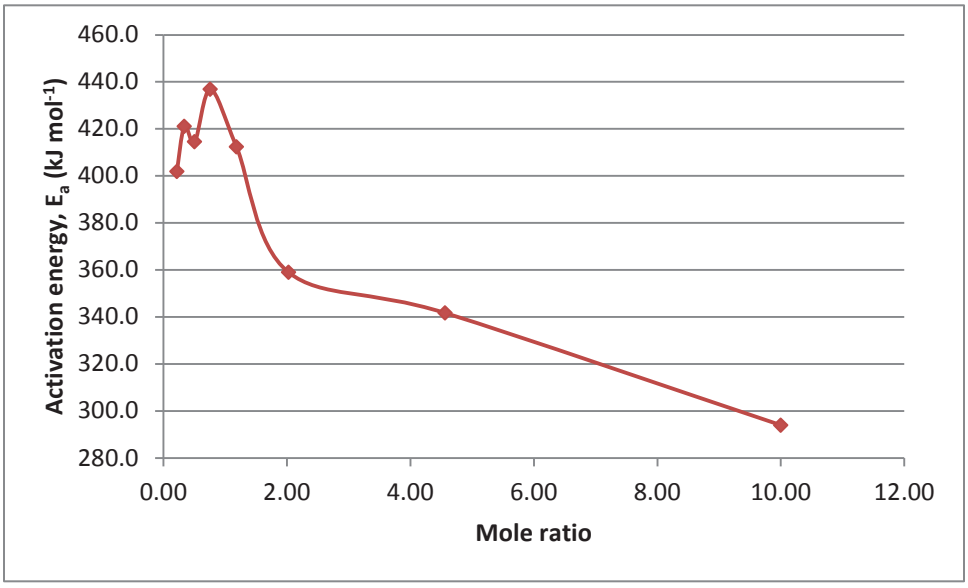


**Figure 22: Activation energies of $n^{th}$ order reactions for peak 2 versus mole ratios of Glutamic acid samples**

**Glutamic acid (FFT):**

The PSI plots with temperature, T (K) on x-axis and $\frac{d\alpha}{dt}$ ($°C^{-1}$) on y-axis for all the samples of Glutamic acid were smoothened using 5 FFT method in the MATLAB software. The smoothened plots of all the samples of Glutamic acid were overlaid as shown in the following figure:

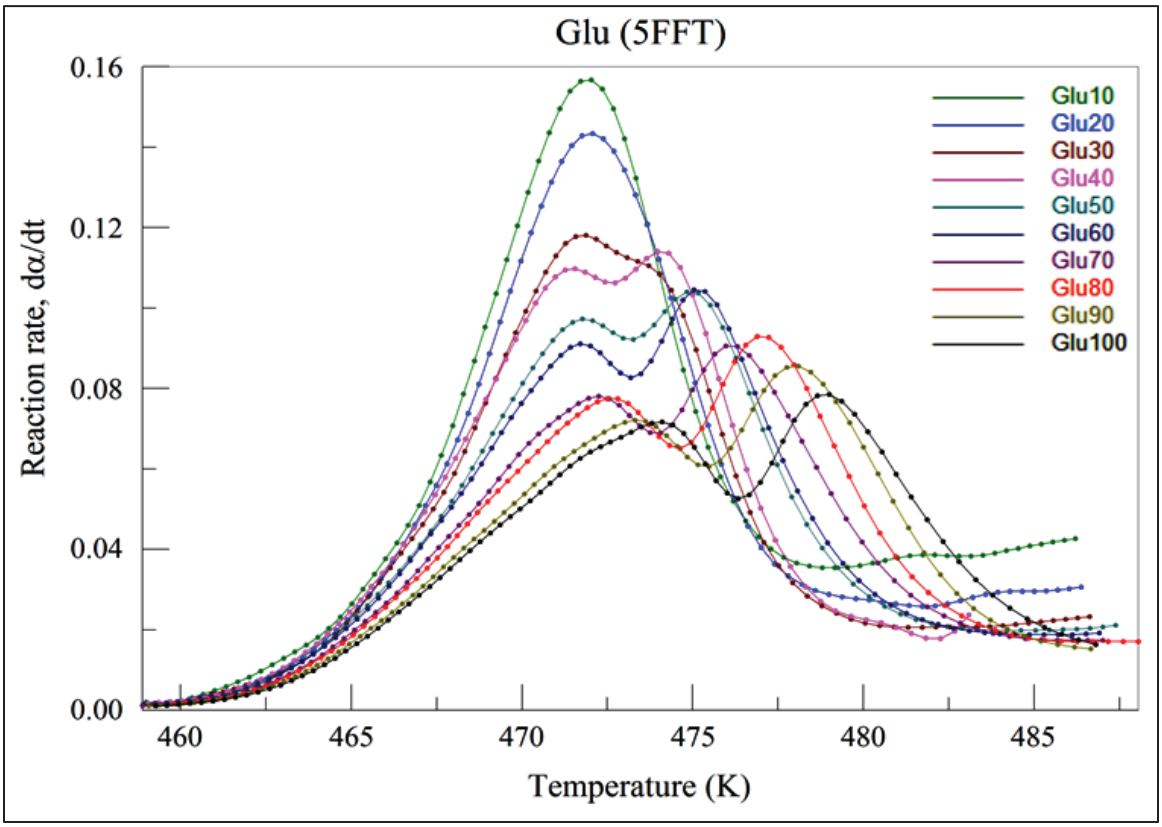


**Figure 23: Overlay of PSI plots of reaction rate profiles of Glutamic acid samples versus temperature**

From these plots, the variables like $T_m$ and $\left(\frac{d\alpha}{dt}\right)_m$ were determined, which correspond to the values at the peak maximum of the peaks of all the samples of

Glutamic acid. The $T_m$ and $\left(\frac{d\alpha}{dt}\right)_m$ values obtained for all the ten samples of Glutamic acid are tabulated below:

**Table 14: Thermogravimetric experimental parameters of Glutamic acid samples after FFT smoothing of PSI plots**

| Sample (5 FFT) | $T_m$ (K) | | $\left(\frac{d\alpha}{dt}\right)_m$ ($K^{-1}$) | |
|---|---|---|---|---|
| | Peak1 | Peak2 | Peak1 | Peak2 |
| **Glu10** | 472.0 | - | 0.157 | - |
| **Glu20** | 472.1 | - | 0.143 | - |
| **Glu30** | 471.9 | 474.0 | 0.118 | 0.108 |
| **Glu40** | 471.6 | 474.0 | 0.110 | 0.114 |
| **Glu50** | 471.8 | 474.8 | 0.097 | 0.104 |
| **Glu60** | 471.7 | 475.0 | 0.091 | 0.105 |
| **Glu70** | 472.2 | 476.0 | 0.078 | 0.091 |
| **Glu80** | 472.5 | 477.2 | 0.078 | 0.093 |
| **Glu90** | 473.3 | 478.1 | 0.072 | 0.086 |
| **Glu100** | 474.1 | 479.0 | 0.072 | 0.079 |

The $T_m$ and $\left(\frac{d\alpha}{dt}\right)_m$ values obtained in the above table were substituted in the equations given in the theory in order to calculate the kinetic parameters like activation energy $(E_a)$, pre-exponential factor $(A)$ and order of the reaction $(n)$ for each sample. The $E_a$ and $A$ values were calculated using equations (15) and (16) for the first order

reaction kinetics and equations (25) and (26) for the $n^{th}$ – order reaction kinetics of each sample. The $n$ value for each sample was calculated by using the equation (28) given in the theory. The calculated values of kinetic parameters for all the samples of Glutamic acid are shown in Table 15. The activation energies ($E_a$) obtained for both peak 1 and peak 2 of Glutamic acid samples were plotted against the mole ratios of those samples, for both first order and $n^{th}$ order kinetics, with the mole ratio on x-axis and $E_a$ on y-axis.

**Table 15: Kinetic parameters of Glutamic acid samples calculated from the TGA data after FFT smoothing of PSI plots**

| Sample 5 FFT | First Order Kinetics | | | | *n* - value | | $n^{th}$ Order Kinetics | | | |
|---|---|---|---|---|---|---|---|---|---|---|
| | $E_a$ (kJ $mol^{-1}$) | | A ($min^{-1}$) | | | | $E_a$ (kJ $mol^{-1}$) | | A ($min^{-1}$) | |
| | Peak 1 | Peak 2 | Peak 1 | Peak 2 | Peak 1 | Peak 2 | Peak 1 | Peak 2 | Peak 1 | Peak 2 |
| **Glu10** | 789.1 | - | 1.49E+86 | - | 1.1 | - | 818.6 | - | 2.83E+89 | - |
| **Glu20** | 722.2 | - | 5.34E+78 | - | 1.0 | - | 738.0 | - | 3.06E+80 | - |
| **Glu30** | 594.3 | 550.5 | 3.29E+64 | 2.26E+59 | 1.4 | 0.4 | 701.0 | 389.2 | 2.51E+76 | 2.69E+41 |
| **Glu40** | 551.3 | 578.8 | 5.81E+59 | 3.16E+62 | 2.0 | 0.4 | 809.6 | 389.8 | 3.50E+88 | 3.13E+41 |
| **Glu50** | 488.9 | 529.9 | 6.01E+52 | 9.33E+56 | 2.5 | 0.5 | 833.2 | 395.5 | 1.33E+91 | 1.14E+42 |
| **Glu60** | 458.1 | 533.0 | 2.22E+49 | 1.90E+57 | 2.5 | 0.6 | 777.4 | 412.7 | 8.53E+84 | 8.81E+43 |
| **Glu70** | 393.2 | 463.9 | 1.08E+42 | 3.32E+49 | 2.8 | 0.7 | 723.6 | 387.6 | 7.03E+78 | 1.17E+41 |
| **Glu80** | 391.1 | 477.2 | 5.96E+41 | 7.06E+50 | 2.8 | 0.5 | 712.6 | 358.7 | 3.78E+77 | 5.74E+37 |
| **Glu90** | 365.1 | 441.7 | 6.32E+38 | 7.01E+46 | 3.0 | 0.6 | 690.5 | 339.0 | 9.84E+74 | 3.25E+35 |
| **Glu100** | 364.2 | 407.1 | 4.38E+38 | 8.74E+42 | 2.2 | 0.4 | 562.4 | 284.9 | 4.63E+60 | 2.89E+29 |

The resulting plots of all glutamic acid samples (FFT) were shown below:

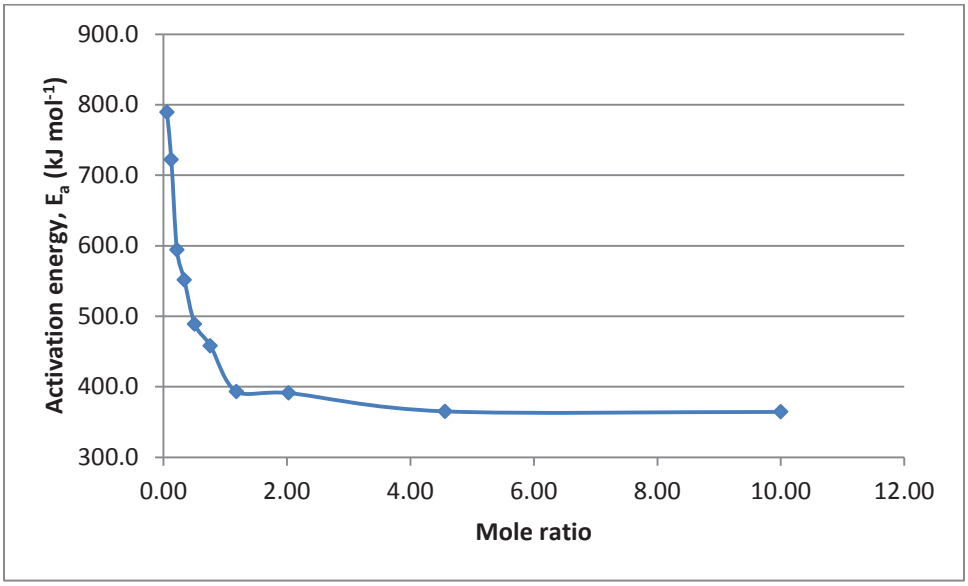


**Figure 24: Activation energies of first order reactions for peak 1 versus mole ratios of Glutamic acid samples after FFT smoothing of PSI plots**

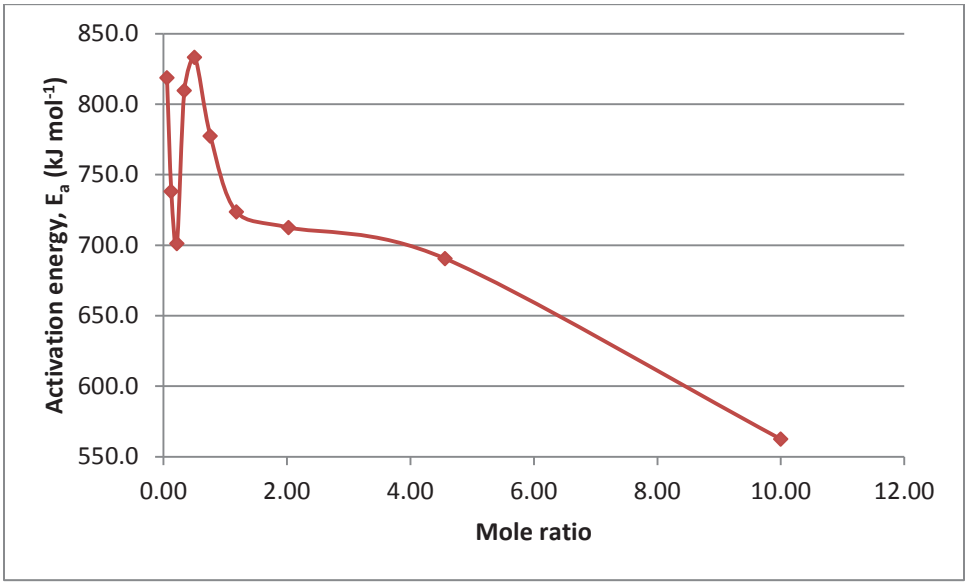


**Figure 25: Activation energies of $n^{th}$ order reactions for peak 1 versus mole ratios of Glutamic acid samples after FFT smoothing of PSI plots**

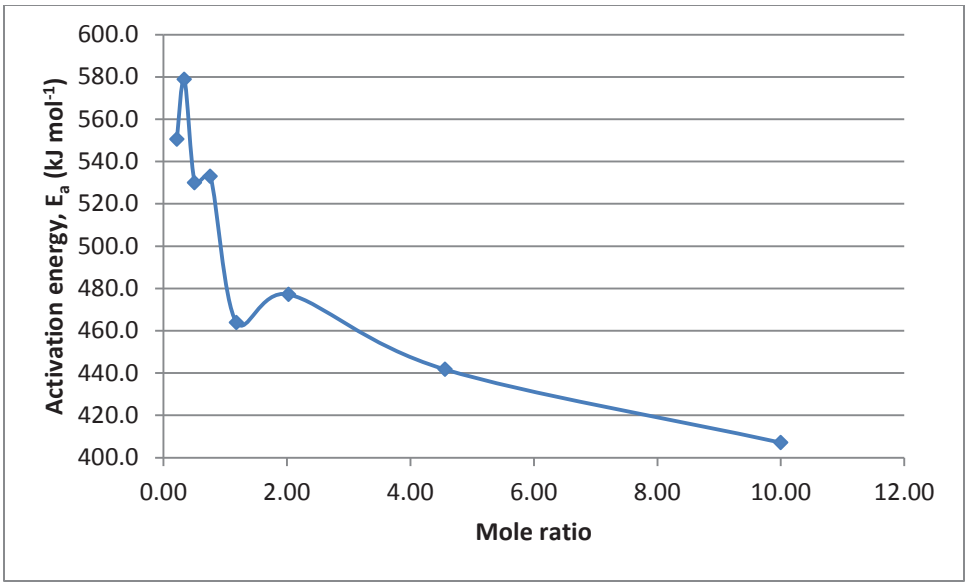


**Figure 26: Activation energies of first order reactions for peak 2 versus mole ratios of Glutamic acid samples after FFT smoothing of PSI plots**

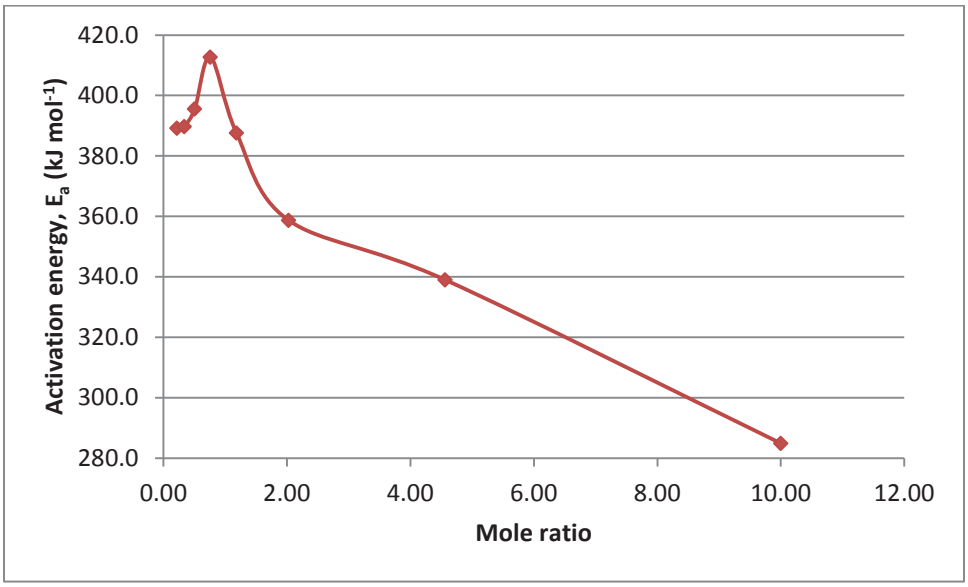


**Figure 27: Activation energies of $n^{th}$ order reactions for peak 2 versus mole ratios of Glutamic acid samples after FFT smoothing of PSI plots**

## Differential Scanning Calorimetry:

The differential scanning calorimetric experiments were carried out for all the samples of Aspartic and Glutamic acids for a better comparison with their TGA data.

### Aspartic acid:

The DSC curves obtained for all the aspartic acid samples were overlaid as shown in Figure 28. From these curves, the differential scanning calorimetric data like heat flow (W/g) and heat output (J/g) and temperature at peak maximum ($T_{max}$) were obtained by analyzing the DSC curves in "Universal Analysis" software provided by TA Instruments. These values are shown in Table 16.

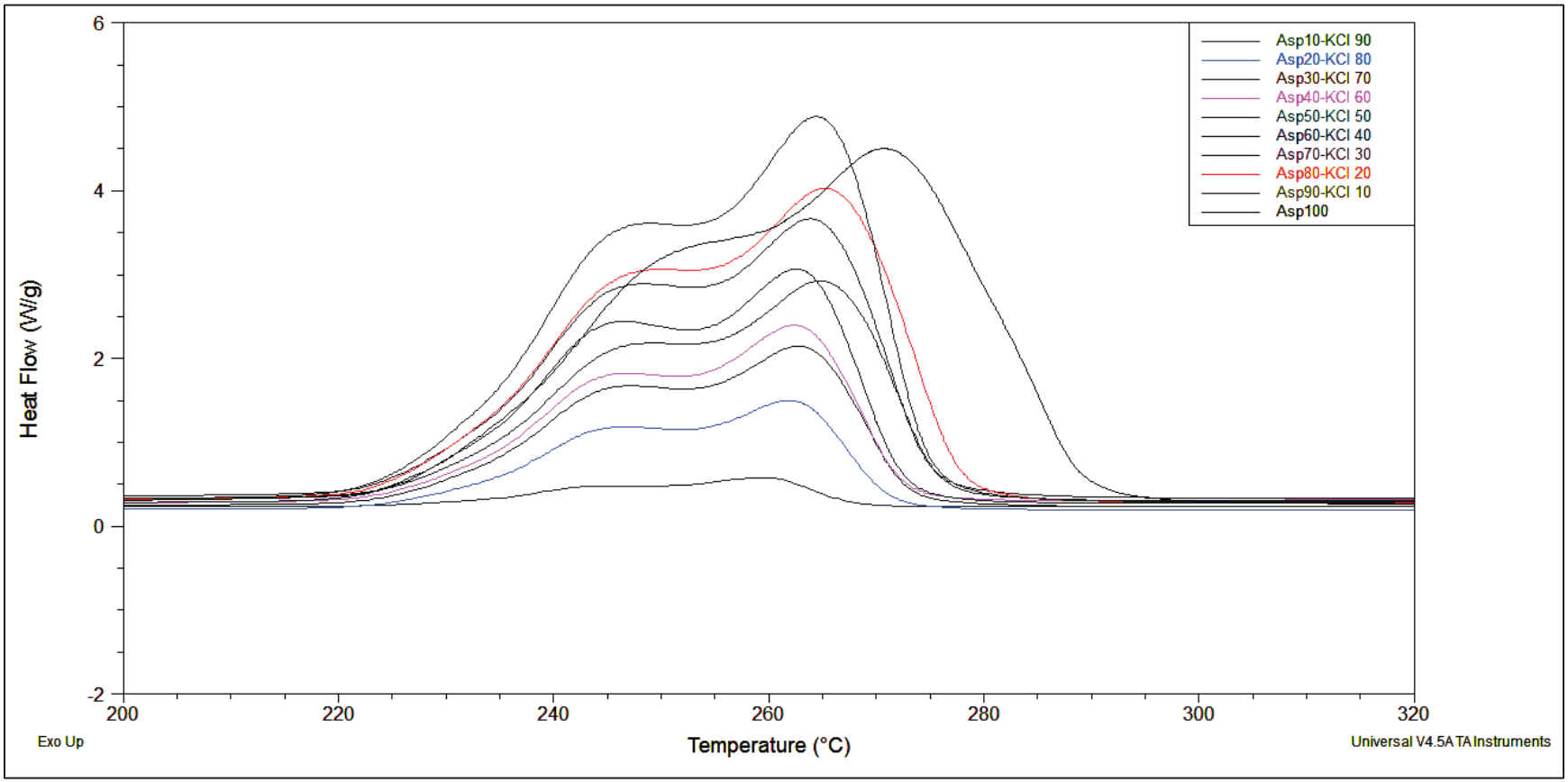


**Figure 28: Overlay of DSC plots of Aspartic acid samples showing heat flow versus temperature**

**Table 16: Differential scanning calorimetric data of Aspartic acid samples**

| Sample | Temperature at peak maximum, $T_{max}$ (°C) | Temperature at peak maximum, $T_{max}$ (K) | Heat Flow (W/g) | Heat Output (J/g) |
|---|---|---|---|---|
| **Asp10** | 259.3 | 532.3 | 0.34 | 48.7 |
| **Asp20** | 261.9 | 534.9 | 1.28 | 203.3 |
| **Asp30** | 262.7 | 535.7 | 1.87 | 308.8 |
| **Asp40** | 262.4 | 535.4 | 2.06 | 330.8 |
| **Asp50** | 264.8 | 537.8 | 2.58 | 442.7 |
| **Asp60** | 262.6 | 535.6 | 2.75 | 463.4 |
| **Asp70** | 263.9 | 536.9 | 3.26 | 571.4 |
| **Asp80** | 265.3 | 538.3 | 3.67 | 672.5 |
| **Asp90** | 264.4 | 537.4 | 4.52 | 777.4 |
| **Asp100** | 270.8 | 543.8 | 4.14 | 884.2 |

The DSC profiles look similar to the derivative thermogravimetric curves, with the reactions occurring in the temperature range of 480 -580 K, approximately close to the thermogravimetric range. The DSC curves of Aspartic acid samples are exothermic peaks with a peak maximum temperature of 543.8 K for Asp100 and 432.3 K for Asp10. Initially, autocatalysis occurs resulting in the formation of polyaspartic acid (PAA) which readily undergoes dehydration and polymer-analogous transformation to form polysuccinimide (PSI) [20]. The heat flow of Asp100 is 4.14 W/g which gradually

decreased to a value of 0.34 W/g in Asp10 as the KCl percentage increased to 90%. Similarly, the heat output of Asp100 is 884.2 J/g which gradually decreased to 48.7 J/g in Asp10.

**Glutamic acid:**

The DSC curves obtained for all the glutamic acid samples were overlaid as shown in Figure 29. From these curves, the differential scanning calorimetric data like heat flow (W/g) and heat output (J/g) and temperature at peak maximum ($T_{max}$) were obtained by analyzing the DSC curves in "Universal Analysis" software provided by TA Instruments. These values are shown in Table 17.

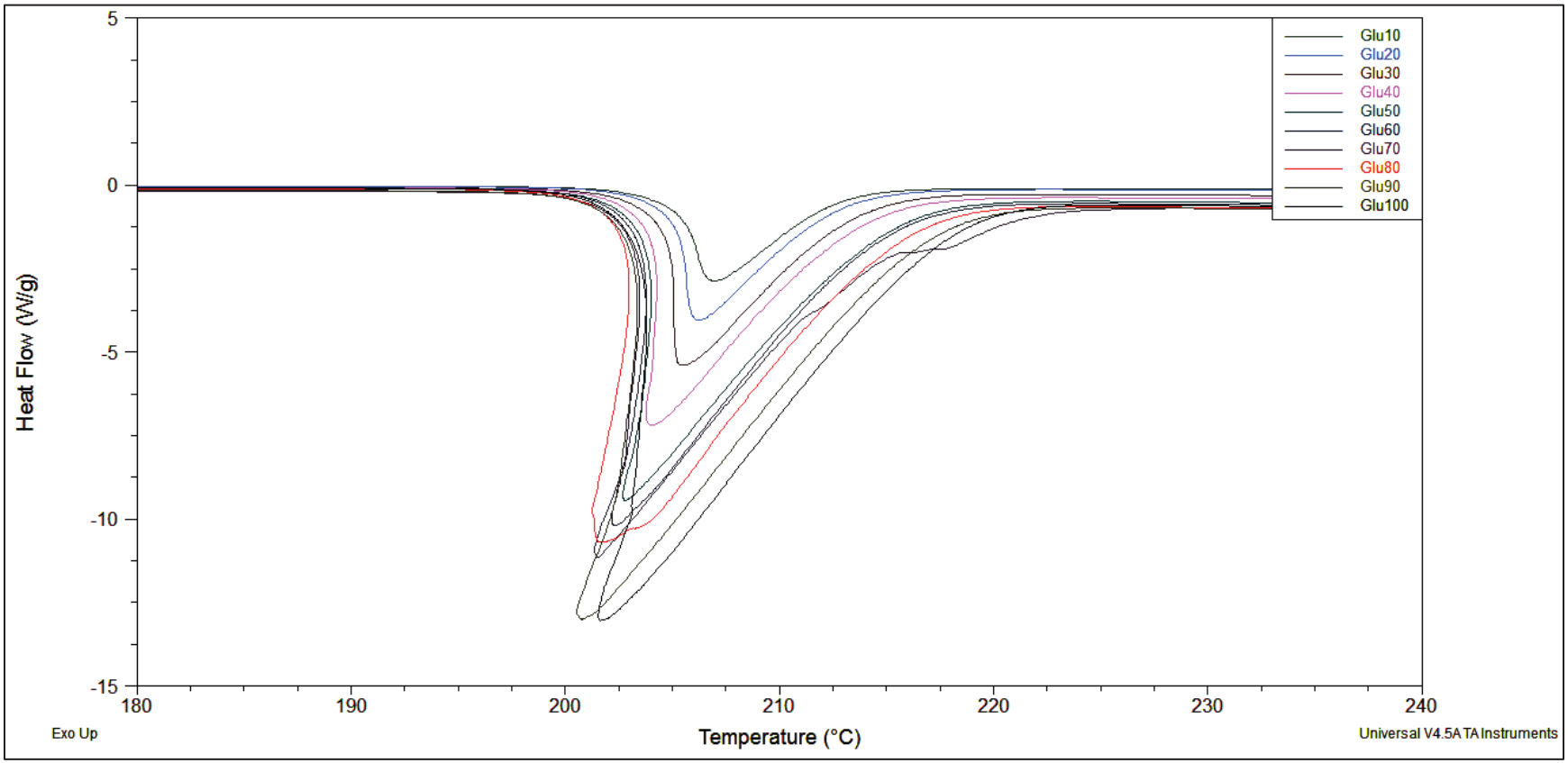


**Figure 29: Overlay of DSC plots of Glutamic acid samples showing heat flow versus temperature**

**Table 17: Differential scanning calorimetric data of Glutamic acid samples**

| Sample | Temperature at peak maximum, $T_{max}$ (°C) | Temperature at peak maximum, $T_{max}$ (K) | Heat Flow W/g | Heat Output J/g |
|---|---|---|---|---|
| **Glu10** | 206.9 | 479.9 | -2.87 | 88.5 |
| **Glu20** | 206.2 | 479.2 | -4.05 | 124.8 |
| **Glu30** | 205.4 | 478.4 | -5.40 | 183.1 |
| **Glu40** | 204.0 | 477.0 | -7.19 | 254.8 |
| **Glu50** | 202.8 | 475.8 | -9.93 | 352.7 |
| **Glu60** | 202.3 | 475.3 | -10.18 | 392.7 |
| **Glu70** | 201.5 | 474.5 | -10.66 | 452.2 |
| **Glu80** | 201.7 | 474.7 | -10.69 | 502.9 |
| **Glu90** | 200.8 | 473.8 | -13.00 | 566.1 |
| **Glu100** | 201.6 | 474.6 | -13.03 | 599.7 |

The DSC curves of Glutamic acid samples are endothermic peaks with a peak maximum temperature of 474.6 K for Asp100 and 479.9 K for Glu10. The heat flow of Glu100 is -13.03 W/g which gradually increased to a value of -2.87 W/g in Glu10, as the KCl percentage increased to 90%. Similarly, the heat output of Glu100 is 599.7 J/g which gradually decreased to 88.5 J/g in Asp10. The DSC endotherm occurs in the temperature range of about 470 – 480 K which corresponds to the initial weight losses of Glutamic acid samples occurring in the same temperature range of about 470 - 480 K. This is also

the melting range of Glutamic acid samples. Therefore, the phase transformation, dehydration and melting can be represented by the DSC endothermic curves. Initially, the phase transformation of $\alpha$ polymorph to $\beta$ polymorph occurs followed by melting, which is further followed by decomposition [1].

The DSC experiments were performed on all the aspartic and glutamic acid samples. But, much analysis was not done on the DSC results obtained in this study. Hence, the DSC results are included but these are not discussed in detail.

# Discussion

## Thermogravimetric Analysis:

### Aspartic acid:

From Figure 14, the heights of both the peaks 1 (at 509.6 K for Asp100) and 2 (at 531.9 K for Asp100) of all the Aspartic acid samples gradually increased, as the KCl concentration increased in the Aspartic acid samples from Asp100 through Asp10 with the peak maximum shifting towards the lower temperature.

From Table 5, the average *n* value for peak 1 of all Aspartic acid samples is 9.2. Therefore, *n* = 9 and thus, the reaction occurring at peak 1 of all aspartic acid samples follows ninth order kinetics. On the other hand, the average *n* value for peak 2 of all Aspartic acid samples is 0.5. Therefore, *n* = 1 and thus, the reaction occurring at peak 2 of all aspartic acid samples follows first order kinetics. The activation energy (when n = 9) of Asp100 is 460.3 kJ $mol^{-1}$ for the reaction occurring at peak 1 and this value gradually increased to 744.2 kJ $mol^{-1}$ in Asp10. Similarly, the activation energy (when n = 1) of Asp100 is 197.6 kJ $mol^{-1}$ for the reaction occurring at peak 2 and this value gradually increased to 253.4 kJ $mol^{-1}$ in Asp10. The gradual variation in the pre-exponential factor values was also observed. From Table 6, the initial weight loss of sample in Asp100 is 26.75 % and as the percentage amount of KCl increased, the initial weight loss decreased gradually to a value of 4.47 % in Asp10. As the KCl concentration in the sample increases, the reaction rate reaches its maximum value at lower temperatures, as observed in Figure 14.

In the aspartic acid samples, a condensation reaction occurs between any two aspartic acid molecules, where an amine and carboxylic acid groups combine to form an amide link with the elimination of one water molecule. Thus, the further reactions occurring at peak 1 and peak 2 of aspartic acid samples do not occur in the solid state. The oxygen atoms of carbonyl and carboxylate groups and nitrogen atom of amino group of aspartic acid are the electronegative groups which can bind with potassium ions by their nucleophilic attack, donating the extra pair of electrons. For the reactions occurring at Peak 1 and Peak 2, the sharp increase in the activation energy values was observed when the mole ratio of the Aspartic acid samples was close to 1:1 (starting from Asp70, followed by Asp60 and Asp50). This can be attributed to the formation of aspartic acid - potassium ion ($K^+$) complex when the amino acid ligands and $K^+$ ions are in equilibrium. The relative equilibrium competition of amino acid with metal ions controls the formation of amino acid – alkali metal complex [51]. Thus, the ratio of number of moles of $K^+$ (alkali metal ion) ions to the number of binding sites of aspartic acid (amino acid ligand) is responsible for the formation of amino acid – metal ion complex, by the binding of $K^+$ ion with nitrogen and oxygen atoms, replacing hydrogen atoms of Aspartic acid.

From the conformational analysis of alkali metal complexes of anionic species of aspartic acid, several possible binding modes of aspartic acid ligand with metal ions were proposed. The aspartate forms bi-dentate and tri-dentate complexes with potassium ($K^+$) ions and the bi-dentate complexes are the most stable [50]. According to this study, the metal ion affinity (MIA) for aspartic acid – $K^+$ complexes are in the range of 439.91-522.62 kJ $mol^{-1}$ [50], which are close to the activation energy values of peak 1 for $n^{th}$

order kinetics, which are in the range of 460.3-744.2 kJ $mol^{-1}$. However, both the studies were carried out in completely different phases and could not be compared.

Using the binding modes specified in the previous paragraph, the three dimensional molecular models of aspartic acid - $K^+$ ion complexes were drawn with the software program ChemBioDraw3D Ultra version 12.0 from Cambridge Software Corporation. The three dimensional models were constructed with their geometry optimized and energy minimized. In these molecular models, the numbering of carbon (C) atoms and oxygen (O) atoms was given according to the numbering specified in the literature [50]. The following figure illustrates different binding modes of $K^+$ ion to aspartic acid ligand:

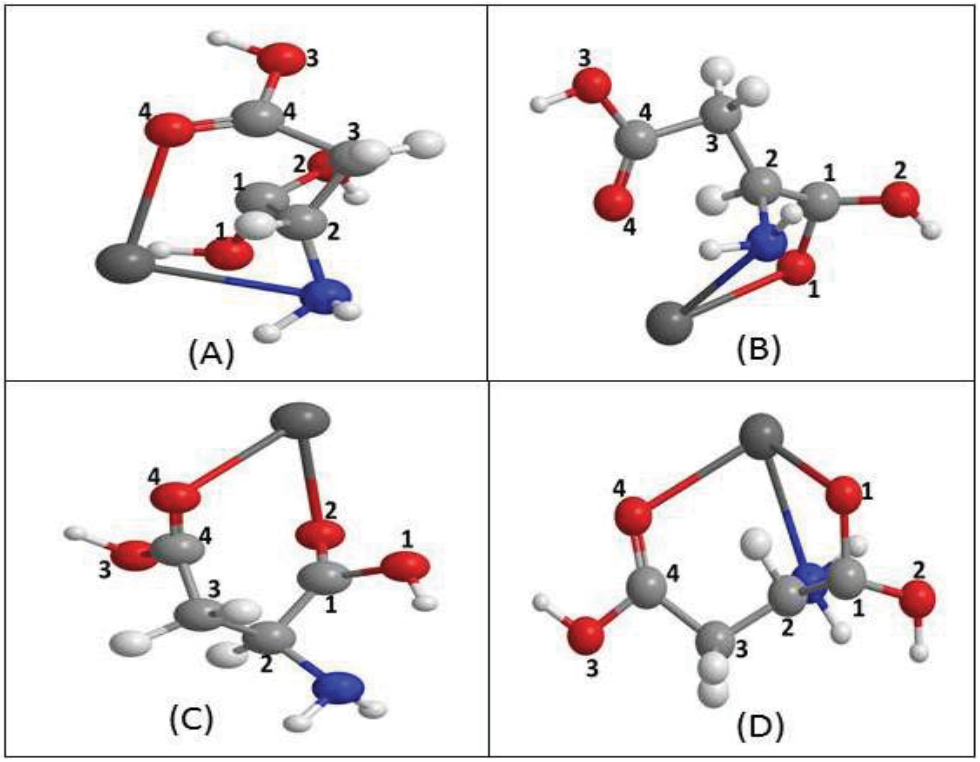


**Figure 30: Different binding modes of $K^+$ ion to aspartic acid ligand**

In the above ball and stick models, each colored ball represent the corresponding element as shown below:

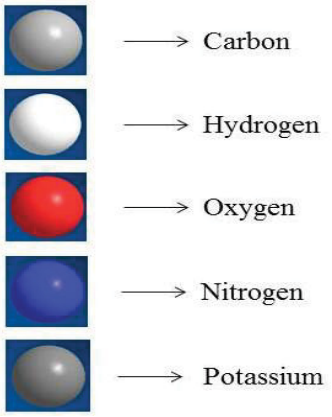


The potassium ion binds to different atoms of aspartic acid in each structure shown in figure 30. The following table gives information on the atoms of aspartic acid to which the $K^+$ ion binds:

**Table 18: The atoms to which $K^+$ ion binds in Aspartic acid structures**

| Structure | Atoms in Aspartic acid |
|---|---|
| A | O4, N |
| B | O1, N |
| C | O2, O4 |
| D | O1, O4, N |

In Figure 30, structures (A), (B), and (C) are the possible bi-dentate complexes of aspartic acid with $K^+$ ion and structure (D) is the possible tri-dentate complex. The gradual increase in the kinetic parameters and decrease in the initial weight loss of

sample in Aspartic acid samples was observed, as the mole ratio of amino acid to KCl gets closer to 1:1. From the *n* values, it is evident that the reaction occurring at peak 1 in all aspartic acid samples corresponds to the formation of polyaspartic acid (PAA) due to autocatalytic chain growth and the reaction occurring at peak 2 corresponds to the formation of polysuccinimide (PSI) due to dehydration and polymer-analogous transformation [20]. The carbon atom of the amide linkage is electron-deficient and has partial positive charge due to electron withdrawal by the highly electronegative double bonded oxygen atom. Thus, the carbon atom becomes susceptible to nucleophile attack by the nitrogen atom of amine group. The nitrogen atom binds with the oxygen atom of amide group along with the removal of water molecule and further cyclization process resulting in the formation of a succinic ring structure [55]. Due to the presence of $K^+$ ions, the nucleophilic attack of nitrogen atom is more on the $K^+$ ions rather than the oxygen atom of the amide group. However, few amino acid molecules undergo further decomposition reactions, but with higher activation energies. Thus, the activation energy $(E_a)$ values gradually increased as the KCl concentration increased from Asp100 through Asp10. The detailed information on the formation of aspartic acid – $K^+$ ion complexes and further decomposition reactions occurring in the aspartic acid samples is not available. Further studies are required to obtain this information.

The ball and stick models of aspartic acid, polyaspartic acid and polysuccinimide are shown below:

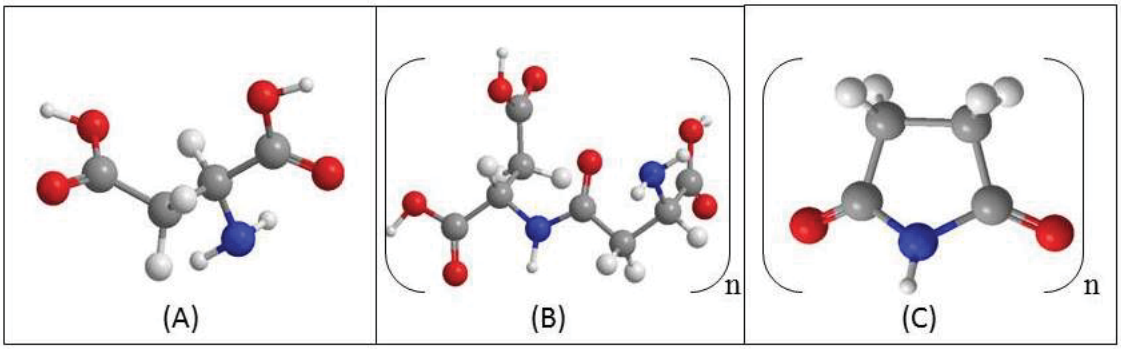


**Figure 31: Ball and stick models of (A) Aspartic acid, (B) Polyaspartic acid and (C) Polysuccinimide**

The overall thermal decomposition reactions occurring in the aspartic acid samples are shown in the following figures:

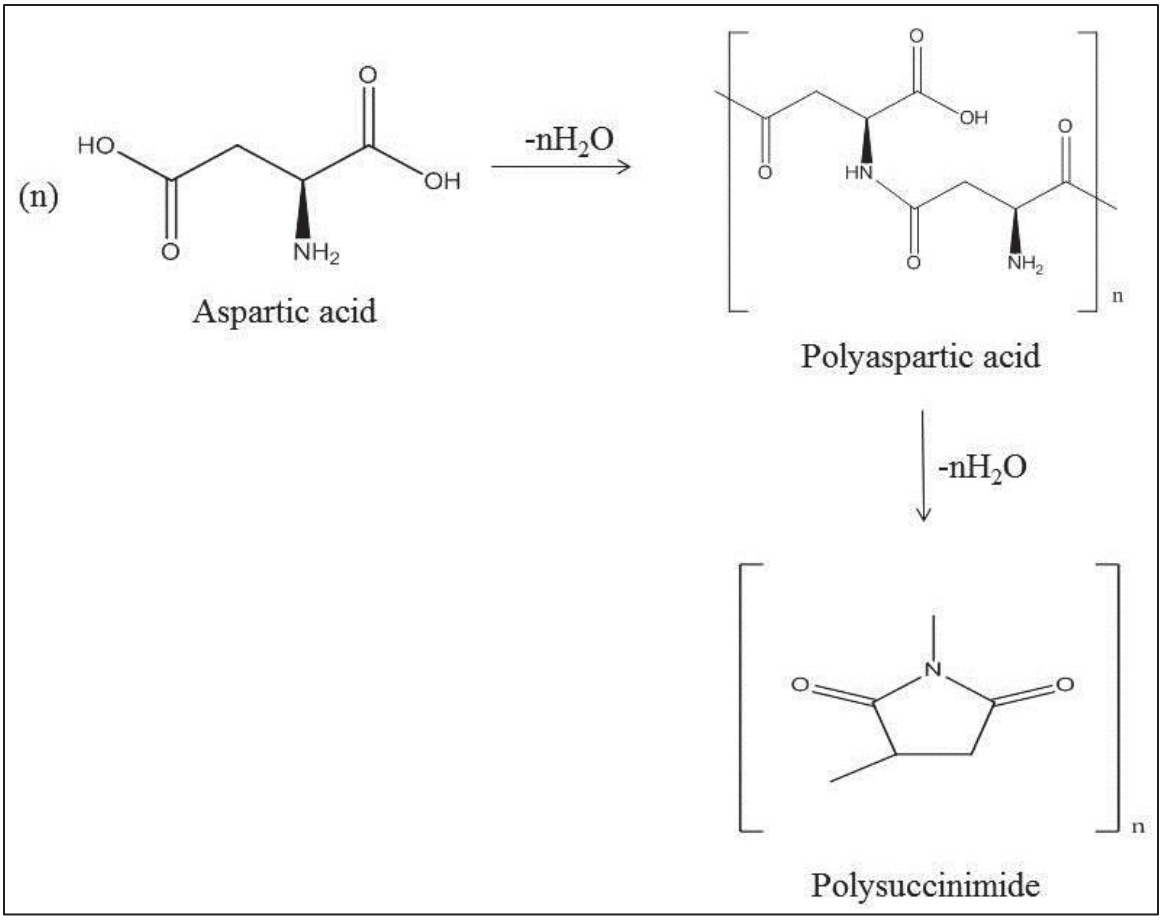


**Figure 32: Thermal decomposition reactions of aspartic acid samples**

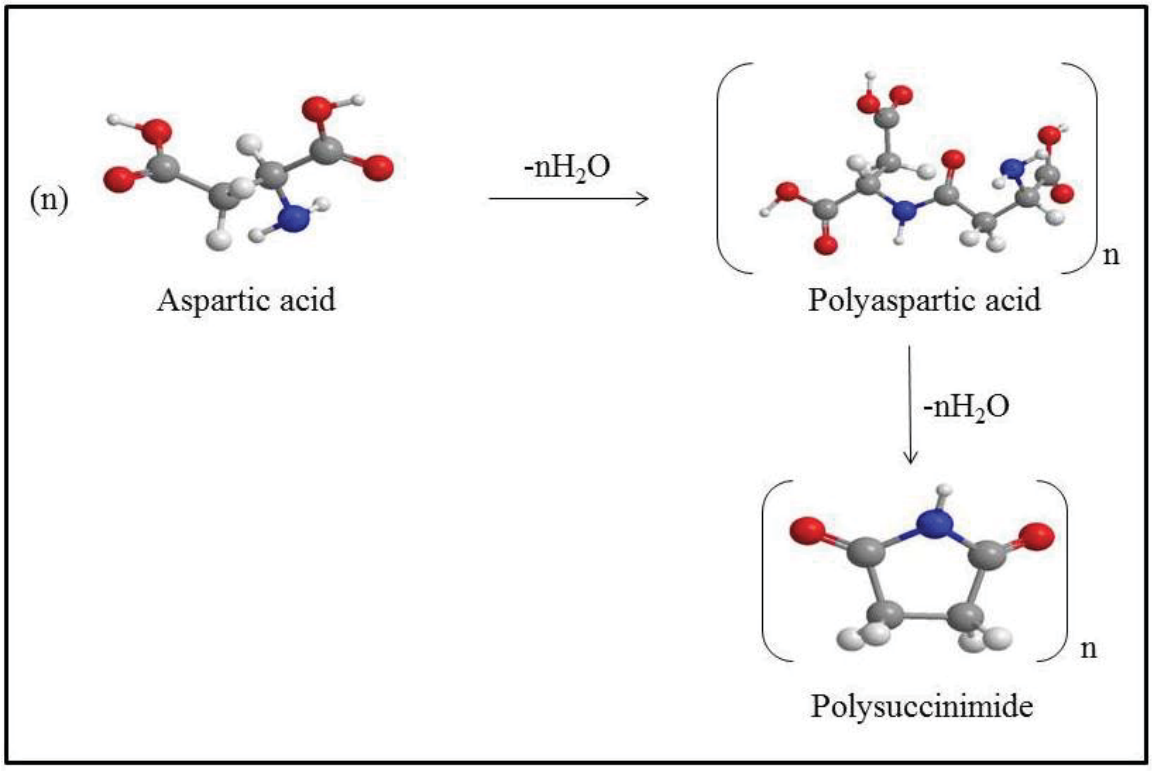


**Figure 33: Ball and stick models of compounds involved in thermal decomposition reactions of aspartic acid samples**

**Glutamic acid:**

The results obtained for Glutamic acid samples are different from that of the Aspartic acid samples. From Figure 23, the heights of both the peaks 1 (at 474.4 K for Glu100) and 2 (at 479.0 K for Glu100) of all the Glutamic acid samples gradually increased, as the KCl concentration increased in the Glutamic acid samples from Glu100 through Glu30 with the peak maximum shifting towards the lower temperature. However, in Glu30, the peak 2 slightly dispersed into peak 1; in Glu20 and Glu10, the peak 2 completely dispersed into peak 1 and disappears. Thus, Glu20 and Glu10 samples have only one peak in each.

From Table 11, the average *n* value for peak 1 of all glutamic acid samples is 2.1. Therefore, $n = 2$ and thus, the reaction occurring at peak 1 of all glutamic acid samples follows second order kinetics. On the other hand, the average *n* value for peak 2 of all glutamic acid samples is 0.5. Therefore, $n = 1$ and thus, the reaction occurring at peak 1 of all glutamic acid samples follows first order kinetics. The activation energy (when n = 2) of Glu100 is 578.9 kJ $mol^{-1}$ for the reaction occurring at peak 1 and this value gradually increased to 839.4 kJ $mol^{-1}$ in Glu10. Similarly, the activation energy (when n = 1) of Glu100 is 420.0 kJ $mol^{-1}$ for the reaction occurring at peak 2 and this value gradually increased to 568.3 kJ $mol^{-1}$ in Glu30. The gradual variation in the pre-exponential factor values was also observed. The peak 2 was not observed in Glu20 and Glu10. From Table 12, the initial weight loss of sample in Glu100 is 11.56 % which is close to the literature value of 12% initial weight loss of glutamic acid [1], and as the amount of KCl increased, the initial weight loss decreased gradually to a value of 2.06 % in Glu10.

Same as discussed for aspartic acid samples, in the glutamic acid samples, a condensation reaction occurs between any two glutamic acid molecules, where an amine and carboxylic acid groups combine to form an amide link with the elimination of one water molecule. Thus, the further reactions occurring at peak 1 and peak 2 of glutamic acid samples do not occur in the solid state. The oxygen atoms of carbonyl and carboxylate groups and nitrogen atom of amino group of glutamic acid are the electronegative groups which can bind with potassium ions by their nucleophilic attack, donating the extra pair of electrons. For the reactions occurring at Peak 1 and Peak 2, the sharp increase in the activation energy values was observed when the mole ratio of the Glutamic acid samples was close to 1:1 (starting from Glu70, followed by Glu60 and Glu50). This can be attributed to the formation of glutamic acid - potassium ion ($K^+$) complex formed when the amino acid ligands and $K^+$ ions are in equilibrium. The relative equilibrium competition of amino acid with metal ions controls the formation of amino acid – alkali metal complex [51]. The ratio of number of moles of $K^+$ (alkali metal ion) ions to the number of binding sites of glutamic acid (amino acid ligand) is responsible for the formation of amino acid – metal ion complex, by the binding of $K^+$ ion with nitrogen and oxygen atoms replacing hydrogen atoms of Glutamic acid.

L-Glutamic acid has two conformers $\alpha$ & $\beta$ conformers which are shown in the following figure:

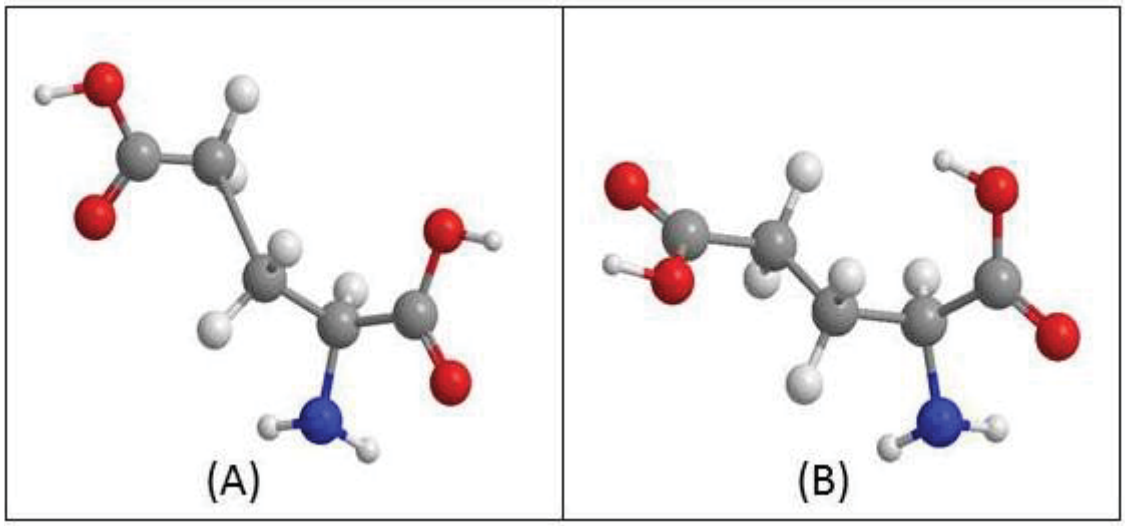


**Figure 34: Ball and stick models of two conformers of L-Glutamic acid**

**(A) $\alpha$ – conformer and (B) $\beta$ – conformer**

Glutamic acid has similar structure as Aspartic acid and the complex properties of both the amino acids are identical [54]. The two amino acids differ in their size. Hence, similar to aspartic acid the three-dimensional models of the possible glutamic acid - $K^+$ ion complexes with optimized geometry and minimized energy were drawn using the software ChemBioDraw3D Ultra (version 12.0). The $K^+$ ion binds in different modes to $\alpha$ & $\beta$ conformers of L-Glutamic acid ligand.

The following figure illustrates different binding modes of $K^+$ ion to $\alpha$ - conformer of glutamic acid ligand:

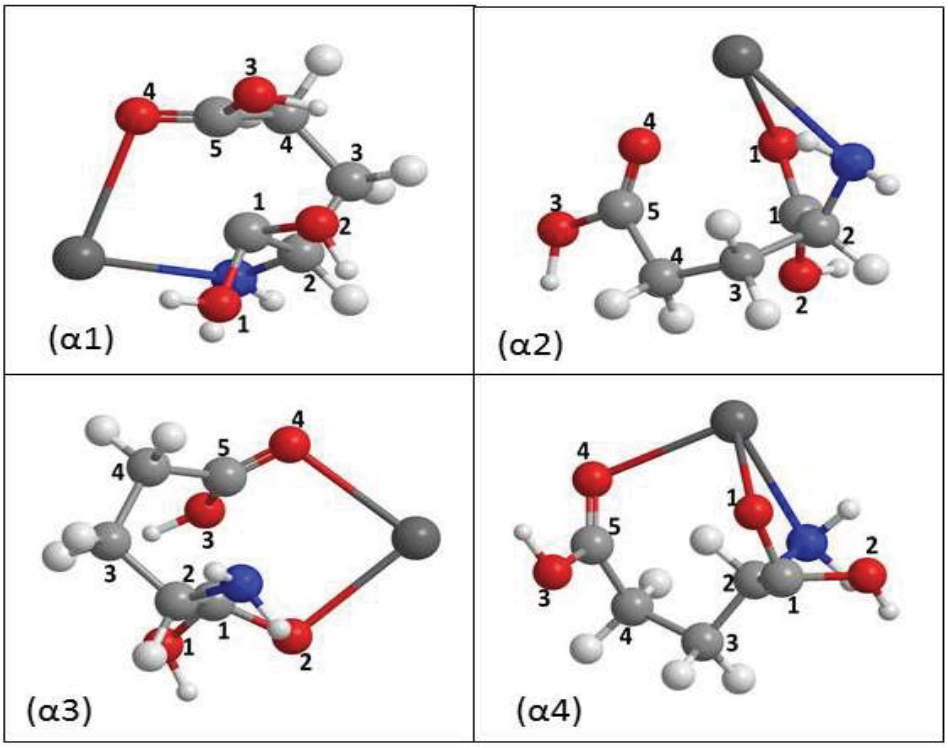


**Figure 35: Different binding modes of $K^+$ ion to α - conformer of glutamic acid ligand**

In the above figure, the structures α1, α2, and α3 are the possible bi-dentate complexes of glutamic acid with $K^+$ ion and structure α4 is the possible tri-dentate complex. The potassium ion binds to different atoms of glutamic acid in each structure shown in figure 35.

The following table gives information on the atoms of $\alpha$ – conformer glutamic acid to which the $K^+$ ion binds:

**Table 19: The atoms to which $K^+$ ion binds in $\alpha$ - conformer of glutamic acid structures**

| Structure | Atoms in $\alpha$ - conformer of glutamic acid |
|---|---|
| α1 | O4, N |
| α2 | O1, N |
| α3 | O2, O4 |
| α4 | O1, O4, N |

The following figure illustrates different binding modes of $K^+$ ion to $\beta$ - conformer of glutamic acid ligand:

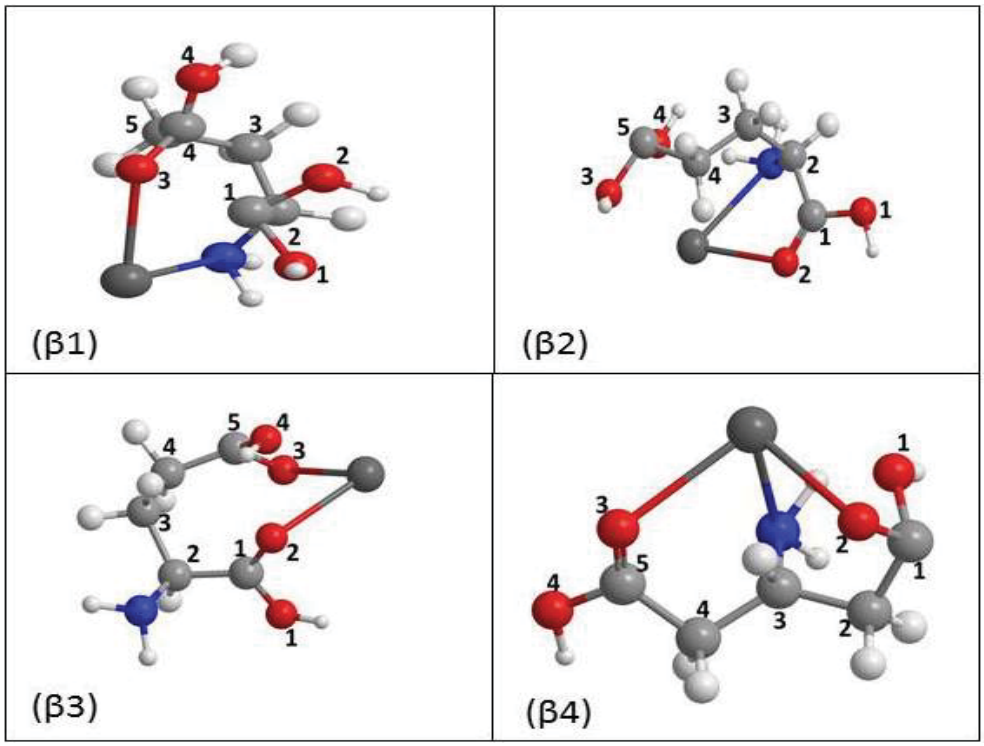


**Figure 36: Different binding modes of $K^+$ ion to $\beta$ - conformer of glutamic acid ligand**

In the above figure, the structures β1, β2, and β3 are the possible bi-dentate complexes of glutamic acid with $K^+$ ion and structure β4 is the possible tri-dentate complex. The potassium ion binds to different atoms of glutamic acid in each structure shown in figure 36.

The following table gives information on the atoms of $\beta$-conformer glutamic acid to which the $K^+$ ion binds:

**Table 20: The atoms to which $K^+$ ion binds in $\beta$ - conformer of glutamic acid structures**

| Structure | Atoms in $\beta$ - conformer of glutamic acid |
|---|---|
| β1 | O3, N |
| β2 | O2, N |
| β3 | O2, O3 |
| β4 | O2, O3, N |

From the phase transformation studies of glutamic acid, at higher temperatures, polymorphic transformation from $\alpha$ to $\beta$ polymorph occurs [1]. The separate TGA profiles of $\alpha$ & $\beta$ polymorphs at a heating rate of 10 °C/min showed that the initial weight loss in $\beta$ polymorph occurred at eight degrees higher temperature when compared to that of $\alpha$ polymorph. The derivative thermogravimetric profile of Glu100 shows two peaks in a temperature range of about five degrees, which is in close agreement with the literature [1]. Thus, the peak 1 of each glutamic acid sample can be attributed to $\alpha$ polymorph and peak 2 can be attributed to $\beta$ polymorph. From Figure 23, the samples Glu100, Glu90 thru Glu40 shows two peaks explaining the transformation of $\alpha$ polymorph to $\beta$ polymorph. As the mole ratio of amino acid : KCl gets closer to 1:1, the reaction rate at peak 2 corresponding to $\beta$ polymorph gradually increases and the peak 2 dispersed partially into peak 1 in Glu30 and completely dispersed into peak 1 in Glu20 and Glu10,

which have a single peak as shown in Figure 23. This suggests that the $\beta$ polymorph partially transforms to $\alpha$ polymorph in Glu30 and completely transforms to $\alpha$ polymorph in Glu20 and Glu10. This can be attributed to the potassium cation interaction with the amino acid ligand to form clusters or complexes [51]. The $K^+$ ion binds with glutamic acid ligand results in the formation of bi-dentate and tri-dentate complexes. As the concentration of KCl in the glutamic acid sample increased, $K^+$ ion forms tri-coordinate complexes with the glutamic acid ligand, which alters the conformation of $\beta$ polymorph to $\alpha$ polymorph, as shown in structure β5 of Figure 36. The carbonyl oxygen atoms binding with potassium ions are far apart in $\beta$ polymorph and in order to form a stable complex with $K^+$ ion, it transforms to $\alpha$ polymorph. Further decomposition can be proposed by a two-step reaction in which pyroglutamic acid (P) is formed due to dehydration and internal cyclization followed by polymerization to form polyglutamic acid (PGA) [1], as shown by black arrows in figures 39 and 40. The carbon atom of the carbonyl group is electron-deficient and has partial positive charge due to electron withdrawal by the highly electronegative double bonded oxygen atom. Thus, the carbon atom becomes susceptible to nucleophile attack by the nitrogen atom of amine group. The nitrogen atom binds with that electron deficient carbon atom, along with the removal of water molecule and further cyclization process resulting in the formation of pyroglutamic acid. Due to the presence of $K^+$ ions, the nucleophilic attack of nitrogen atom is more on the $K^+$ ions rather than the oxygen atom of the amide group. However, few amino acid molecules undergo further decomposition reactions, but with higher activation energies. Thus, the activation energy $(E_a)$ values gradually increased as the KCl concentration increased from Glu100 through Glu10.

The results obtained in this study revealed that, at higher concentrations of KCl, the $\beta$ polymorph transforms to $\alpha$ polymorph. The $\alpha$ polymorph thus formed, undergoes dehydration and internal cyclization to form pyroglutamic acid (P) followed by polymerization to form polyglutamic acid (PGA), as shown by blue arrows in figures 39 and 40. This proposal is based on the results obtained in this study and the earlier studies referenced.

The detailed information on the formation of glutamic acid-potassium ion complexes, conversion of the $\beta$ polymorph to $\alpha$ polymorph and further decomposition reactions occurring in the glutamic acid samples is not available. Further studies are required to obtain this information.

The ball and stick models of glutamic acid, pyroglutamic acid and polyglutamic acid are shown below:

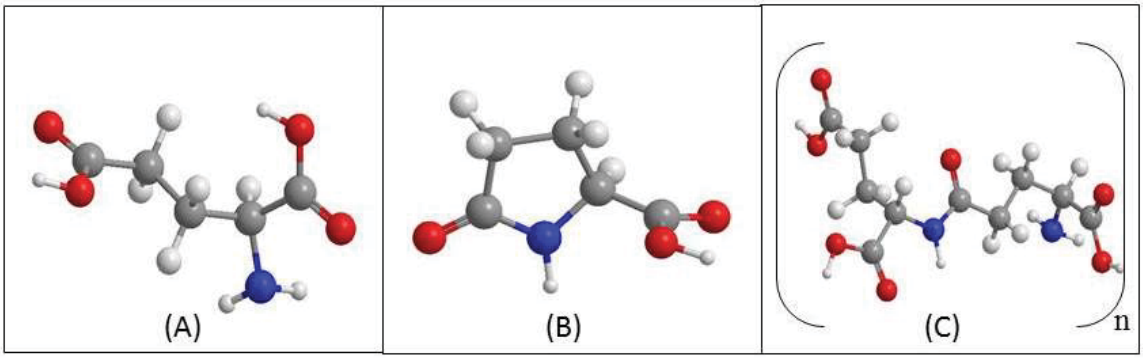


**Figure 37: Ball-stick models of (A) Glutamic acid, (B) Pyroglutamic acid and (C) Polyglutamic acid**

The overall thermal decomposition reactions occurring in the glutamic acid samples are shown in the following figures:

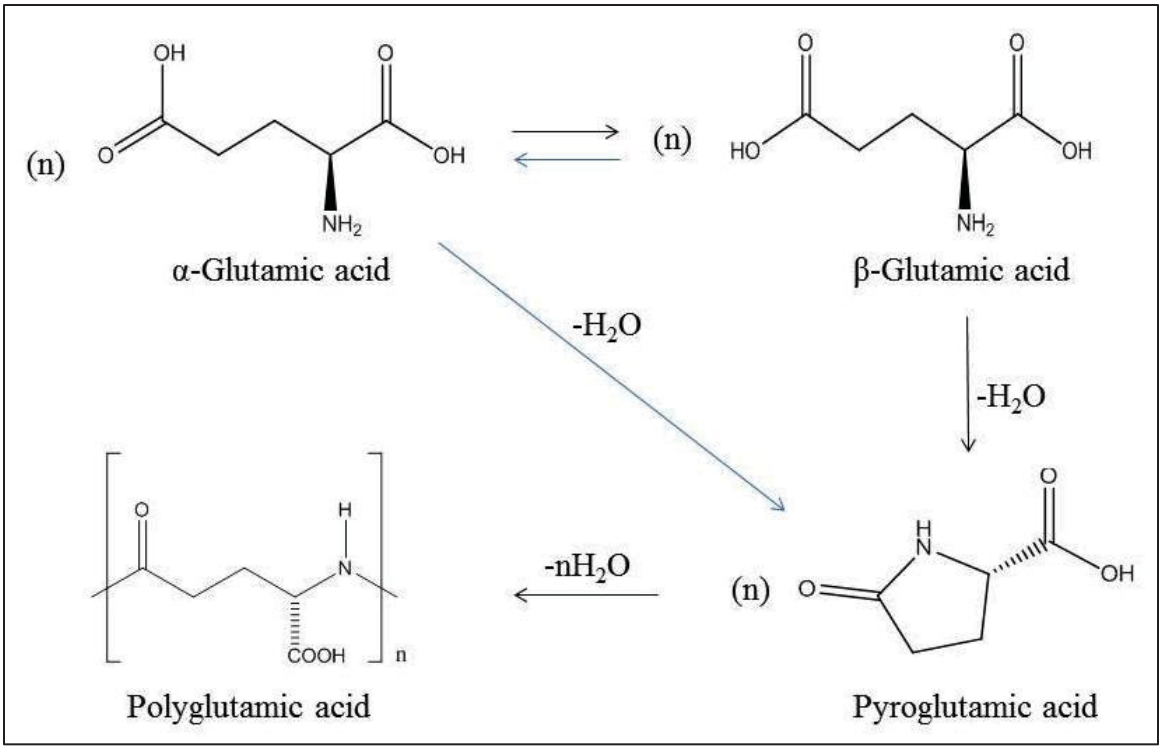


**Figure 38: Thermal decomposition reactions of glutamic acid samples**

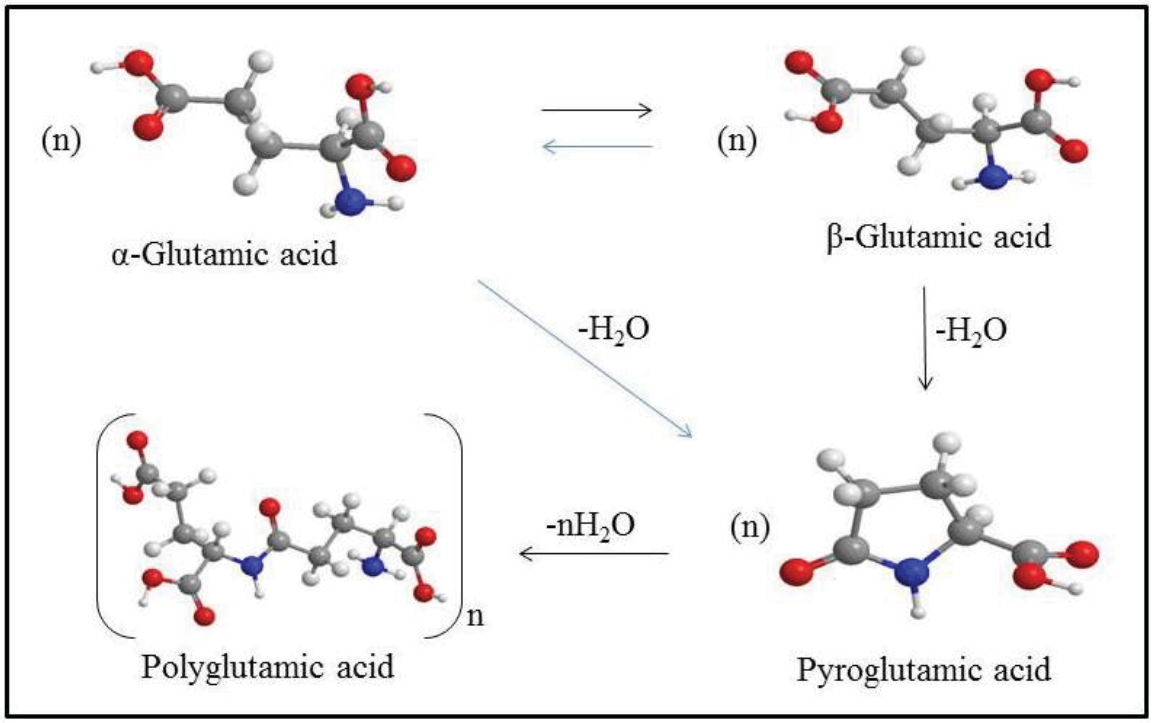


**Figure 39: Ball and stick models of compounds involved in thermal decomposition reactions of glutamic acid samples**

# Conclusion

The thermal analysis of Aspartic and Glutamic acid samples in KCl matrix was performed by using thermo-analytical techniques like thermogravimetric analysis (TGA) and differential scanning calorimetry (DSC). From the thermogravimetric data, the kinetic parameters like activation energy ($E_a$), pre-exponential factor ($A$) and order of the reaction ($n$) for the reactions occurring in each sample were calculated. The results obtained in this study can be attributed to the reactions occurring in these amino acids due to thermal treatment, as proposed in the literature. The results also showed how the potassium ion interaction with amino acid affects the experimental data and kinetic parameters of aspartic and glutamic acid samples in both TGA and DSC. However, the results of glutamic acid samples are different from that of the aspartic acid samples. The interesting observation made in this study is that as the potassium chloride concentration increased in the glutamic acid samples, the $\beta$ polymorph of L-Glutamic acid transforms to $\alpha$ polymorph, which undergoes the further decomposition reactions. In view of the pharmacological importance of the aspartate and glutamate complexes, it is essential to understand their reaction mechanisms. The results obtained in this study can be utilized for the applications involving amino acid based substances and also to understand their thermal stability as well as determining the thermal and kinetic properties.

## References


1. Wu, H., Reeves-McLaren, N., Jones, S., Ristic, R. I., Fairclough, J. P. A., & West, A. R. (2010). Phase Transformations of Glutamic Acid and Its Decomposition Products. *Crystal Growth & Design*, *10*(2), 988–994.
2. Grunenberg, A., Bougeard, D., Schrader, B., & Essen, U. (1984). DSC - Investigation of 22 crystalline neutral aliphatic amino acids in the temperature range 233 to 423 K. *Thermochimica Acta*, *77*, 59–66.
3. Rodante, F., & Marrosu, G. (1990). Thermal analysis of some α-amino acids using simultaneous TG-DSC apparatus. The use of dynamic thermogravimetry to study the chemical kinetics of solid state decomposition. *Thermochimica Acta, 171*, 15–29.
4. Leung, S. S., & Grant, D. J. (1997). Solid state stability studies of model dipeptides: aspartame and aspartyl-phenylalanine. *Journal of pharmaceutical sciences*, *86*(1), 64–71.
5. Tian, F., Sane, S., & Rytting, J. H. (2006). Calorimetric investigation of protein/amino acid interactions in the solid state. *International journal of pharmaceutics*, *310*(1-2), 175–86.
6. Manning, M.C., Patel, K., Borchardt, R.T. (1989). Stability of protein pharmaceuticals. *Pharm. Res. 6*, 903–917.
7. Arakawa, T., Prestrelski, S.J., Kenney, W.C., Carpenter, J.F. (2001). Factors affecting short-term and long-term stabilities of proteins. *Adv. Drug Deliv. Rev. 46*, 307–326.
8. Rodante, F., Fantauzzi, F., & Catalani, G. (1996). Thermal analysis of a series of dipeptides having α-alanine as the first term. Mutual influence of structures. *Thermochimica Acta*, *284*(2), 351–365.

9. Rodante, F., Marrosu, G., & Catalani, G. (1992). Thermal analysis of different series of dipeptides, *Thermochimica Acta*, *197*, 147–160.
10. Olafsson, P. G., & Brynn, a M. (1970). Evaluation of thermal decomposition temperatures of amino acids by differential enthalpic analysis. *Mikrochimica acta*, (5), 871–878.
11. Sharma, R. K., Chan, W. G., Wang, J., Waymack, B. E., Wooten, J. B., Seeman, J. I., & Hajaligol, M. R. (2004). On the role of peptides in the pyrolysis of amino acids. *Journal of Analytical and Applied Pyrolysis*, *72*(1), 153–163.
12. Lee, J. W., Thomas, L. C., & Schmidt, S. J. (2011). Investigation of the heating rate dependency associated with the loss of crystalline structure in sucrose, glucose, and fructose using a thermal analysis approach (Part I). *Journal of agricultural and food chemistry*, *59*(2), 684–701.
13. Badelin, V. G., Kulikov, O. V., Vatagin, V. S., Udzig, E., Zielenkiewicz, A., Zielenkiewicz, W., & Krestov, G. A. (1990). Physico-chemical properties and their solutions of peptides, *Thermochimica Acta*, *169*(August 1989), 81–93.
14. He, L. J., Fan, J. F., & Tang, M. (2010). DFT study of gaseous conformers of aspartic acid. *Journal of Theoretical and Computational Chemistry*, *09*(03), 687–700.
15. Kim, S. K., Ha, T., & Schermann, J.-P. (2010). Biomolecular structures: from isolated molecules to the cell crowded medium. *Physical chemistry chemical physics : PCCP*, *12*(14), 3334–5.
16. Tananaeva, N. N., Gorokhovatskaya, M. Ya., Tikhonova, R. V, & Kostromina, N. A. (1986). Investigation of the conformation of aspartic acid by the NMR method. *Theoretical and Experimental Chemistry*, *21*(4), 493–497.

17. Kumar, A. (2012). Polyaspartic Acid - A Versatile Green Chemical. *Che Sci Rev Lett., 1*(3), 162–167.

18. Shogren, R. L., Willett, J. L., Westmoreland, D., Gonzalez, S. O., Doll, K. M., & Swift, G. (2008). Properties of copolymers of aspartic acid and aliphatic dicarboxylic acids prepared by reactive extrusion. *Journal of applied polymer science*, *110*(6), 3348-3354.

19. Wang, Y., Hou, Y., Ruan, G., Pan, M., & Liu, T. (2003). Study on the polymerization of aspartic acid catalyzed by phosphoric acid. *Journal of Macromolecular Science, Part A*, *40*(3), 293-307.

20. Goldberg, V. M., Lomakin, S. M., Todinova, A. V., Shchegolikhin, A. N., & Varfolomeev, S. D. (2009). Regulation of solid-phase polycondensation of L-aspartic acid. *Doklady Physical Chemistry,* 429*(2),* 252-254.

21. Goldberg, V. M., Todinova, A. V., Shchegolikhin, A. N., & Varfolomeev, S. D. (2011). Kinetic parameters for solid-phase polycondensation of L-aspartic acid: Comparison of thermal gravimetric analysis and differential scanning calorimetry data. *Polymer Science Series B*, *53*(1-2), 10-15.

22. Fouad, E. A., El-Badry, M., Fathalla, D., & Mahmoud, A. Z. (2012). Preparation and investigation of acetyl salicylic acid–glutamic acid complex - A novel oral delivery system. *Digest Journal of Nanomaterials and Biostructures*, *4*(2), 299–308.

23. Cuomo, D., G. Martella, E. Barabino et al. (2009). Metabotropic glutamate receptor subtype 4 selectively modulates both glutamate and GABA transmission in the striatum: implications for Parkinson's disease treatment. *J. Neurochem., 109* (4)1096-1105.

24. Smith, Q. R. (2000). Transport of glutamate and other amino acids at the blood-brain barrier. *J. Nutr., 130*(4), 1016S-1022S.

25. Vlase, T., Vlase, G., Doca, M., & Doca, N. (2003). Specificity of decomposition of solids in non-isothermal conditions. *Journal of thermal analysis and calorimetry*, *72*(2), 597-604.

26. Nunes, R. S., & Cavalheiro, E. T. (2007). Thermal behavior of glutamic acid and its sodium, lithium and ammonium salts. *Journal of Thermal Analysis and Calorimetry*, *87*(3), 627-630.

27. Huang, Y. F., Kuan, W. H., Chiueh, P. T., & Lo, S. L. (2011). A sequential method to analyze the kinetics of biomass pyrolysis. *Bioresource technology, 102*(19), 9241-9246.

28. Vyazovkin, S. (1997), Evaluation of activation energy of thermally stimulated solid-state reactions under arbitrary variation of temperature. *J. Comput. Chem., 18*(3), 393–402.

29. Otero, M., Calvo, L. F., Gil, M. V, Garcia, A. I., & Moran, A. (2008). Co-combustion of different sewage sludge and coal: A non-isothermal thermogravimetric kinetic analysis. *Bioresource technology, 99*(14), 6311–6319.

30. Mackenzie, R. C. (1979). Nomenclature in thermal analysis, part IV. *Thermochimica Acta*, *28*(1), 1-6.

31. Brown, Michael E. (1998). Introduction to Thermal Analysis: Techniques and Applications, London, Chapman & Hall.

32. Giron, D., (2002). Applications of Thermal Analysis and Coupled Techniques in Pharmaceutical Industry. *Journal of Thermal Analysis and Calorimetry, 68*(2), 335-357.
33. Skoog, D. A., Holler, F. J. & Nieman, T. A. (1998). Principles of instrumental analysis, fifth edition, Harcourt Publishers.
34. Keattch, C., (1969). *An Introduction to Thermogravimetry*. Heyden, London.
35. Fahmey, M.A.; Zayed, M.A.; El-Shobaky, H.G. (2005). Study of some phenolic-iodine redox polymeric products by thermal analyses and mass spectrometry, *J. Therm. Anal. Calorim.*, *82*, 137-142.
36. Oswald, H. R., & Wiedemann, H. G. (1977). Factors influencing thermoanalytical curves. *J. Thermal Anal., 12*(2), 147-168.
37. Speyer, R. F. (1994). *Thermal analysis of materials* (Vol. 5). Marcel Dekker, CRC Press.
38. Patton, D.L. (2008). Polymer Techniques PSC341L/720 electronic handout, Polymer Science, University of Southern Mississippi.
39. Haines, P.J., Fifield, F. W. (2000). Thermal method of analysis, *Environmental analytical chemistry,* Malden, MA: Blackwell Science, Oxford, 253-279.
40. Simon, P., & Cibulkova, Z. Measurement of heat capacity by differential scanning calorimetry. 77-80, Slovak university of technology.
41. Lukas, K., & LeMaire, P.K. (2009). Differential scanning calorimetry: fundamental overview. *Resonance, 14*(8):807–17.

42. Chiu, M. H., & Prenner, E. J. (2011). Differential scanning calorimetry: an invaluable tool for a detailed thermodynamic characterization of macromolecules and their interactions. *Journal of Pharmacy and Bioallied Sciences*, *3*(1), 39.

43. McElhaney, R. N. (1982). The use of differential scanning calorimetry and differential thermal analysis in studies of model and biological membranes. *Chemistry and physics of lipids*, *30*(2), 229-259.

44. Schubnell, M. (2000). Temperature and Heat Flow Calibration of A DSC-instrument in the Temperature Range Between− 100 and 160° C. *Journal of thermal analysis and calorimetry*, *61*(1), 91-98.

45. Clas, S., Dalton, C. R., & Hancock, B.C. (1999). Differential scanning calorimetry: Applications in drug development. *Pharma Sci Technol Today, 2*, 311–320.

46. Freire, E. (1995). Differential scanning calorimetry. *Protein stability and folding*, Humana Press, 191-218.

47. TA Instruments. (2009). Thermogravimetric Analysis TGA 2050 user manual & Differential Scanning Calorimetry DSC 2910 user manual.

48. Anasys: Macrothermal analysis, http://www.anasys.co.uk/library/macrota.htm

49. www.cambridgesoft.com/software/ChemDraw

50. Sang-Aroon, W., & Ruangpornvisuti, V. (2008). Conformational analysis of alkali metal complexes of anionic species of aspartic acid, their interconversion and deprotonation: A DFT investigation. *Journal of Molecular Graphics and Modelling*, *26*(6), 982-990.

51. Jang, S., Ju Song, M., Kim, H., & Choi, S. S. (2011). Formation of metal complex ions from amino acid in the presence of $Li^+$, $Na^+$ and $K^+$ by electrospray ionization:

metal replacement of hydrogen in the ligands. *Journal of Mass Spectrometry*, *46*(5), 496-501.

52. Sang-Aroon, W., & Ruangpornvisuti, V. (2007). Conformational analysis of alkali metal complexes of aspartate dianion and their interactions in gas phase. *Journal of Molecular Graphics and Modelling, 26*(1), 342-351.
53. Ketabi, S., Haeri, H. H., & Hashemianzadeh, S. M. (2011). Solvation free energies of glutamate and its metal complexes: A computer simulation study. *Journal of molecular modeling*, *17*(4), 889-898.
54. Sajadi, S. A. (2010). Metal ion-binding properties of L-glutamic acid and L-aspartic acid, a comparative investigation. *Natural Science*, *02* (2010), 85–90.
55. Heaton, A. L., & Armentrout, P. B. (2008). Thermodynamics and mechanism of the deamidation of sodium-bound asparagine. *Journal of the American Chemical Society*, *130*(31), 10227-10232.

# Appendix

The bond distances of potassium ions and binding atoms of aspartic acid molecules in the three-dimensional structures of complexes shown in Figure 30 were determined as shown below:

**Appendix 1: The bond distances of $K^+$ ions and binding atoms of aspartic acid molecules**

| Structure | Bond | Bond distance (Å) |
|---|---|---|
| A | $K^+$ - $O_4$ | 2.670 |
| | $K^+$ - N | 2.706 |
| B | $K^+$ - $O_1$ | 2.670 |
| | $K^+$ - N | 2.706 |
| C | $K^+$ - $O_2$ | 2.681 |
| | $K^+$ - $O_4$ | 2.681 |
| D | $K^+$ - $O_1$ | 2.670 |
| | $K^+$ - $O_4$ | 2.670 |
| | $K^+$ - N | 2.706 |

The bond distances of potassium ions and binding atoms of $\alpha$ - conformers of glutamic acid molecules in the three-dimensional structures of complexes shown in Figure 35 were determined as shown below:

**Appendix 2: The bond distances of $K^+$ ions and binding atoms of $\alpha$ - conformers of glutamic acid molecules**

| Structure | Bond | Bond distance (Å) |
|---|---|---|
| α1 | $K^+$ - $O_4$ | 2.670 |
| | $K^+$ - N | 2.706 |
| α2 | $K^+$ - $O_1$ | 2.670 |
| | $K^+$ - N | 2.712 |
| α3 | $K^+$ - $O_2$ | 2.670 |
| | $K^+$ - $O_4$ | 2.670 |
| α4 | $K^+$ - $O_1$ | 2.670 |
| | $K^+$ - $O_4$ | 2.670 |
| | $K^+$ - N | 2.706 |

The bond distances of potassium ions and binding atoms of $\beta$ - conformers of glutamic acid molecules in the three-dimensional structures of complexes shown in Figure 36 were determined as shown below:

**Appendix 3: The bond distances of $K^+$ ions and binding atoms of *β* - conformers of glutamic acid molecules**

| Structure | Bond | Bond distance (Å) |
|---|---|---|
| β1 | $K^+$ - $O_3$ | 2.666 |
| | $K^+$ - N | 2.705 |
| β2 | $K^+$ - $O_2$ | 2.682 |
| | $K^+$ - N | 2.713 |
| β3 | $K^+$ - $O_2$ | 2.683 |
| | $K^+$ - $O_3$ | 2.672 |
| β4 | $K^+$ - $O_2$ | 2.692 |
| | $K^+$ - $O_3$ | 2.676 |
| | $K^+$ - N | 2.711 |

These bond distances in all the aspartic acid and glutamic acid complexes with optimized geometry and minimized energy were determined in ChemBioDraw3D Ultra (version 12.0) and all these values were in close agreement with those in the most stable conformers, as proposed in the literature [50].